A Double-Walled Flexible Friction-Based Locomotion and Transport Mechanism

S. Treep

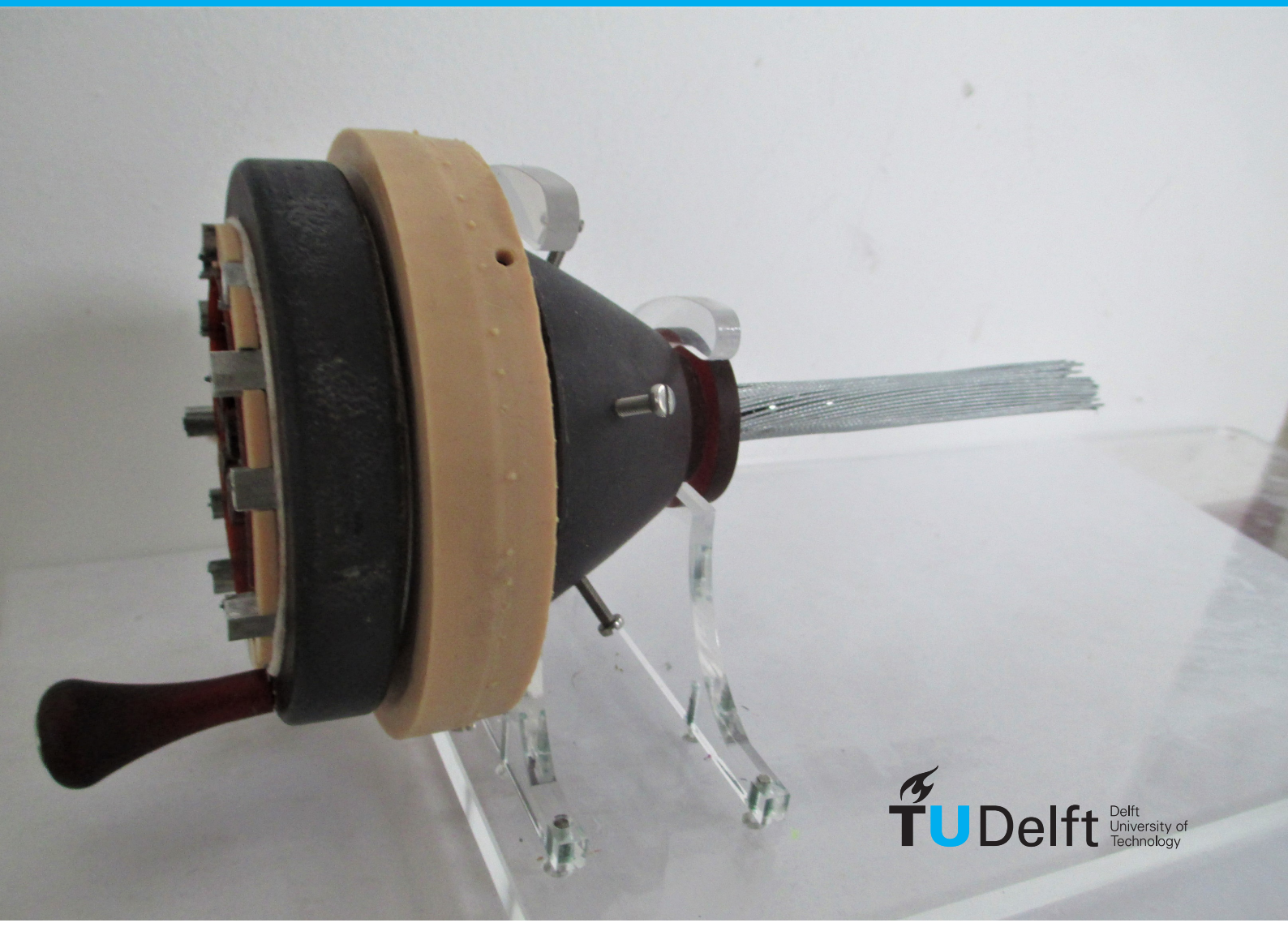

A Double-Walled Flexible Friction-Based Locomotion and Transport Mechanism

by

S. Treep

to obtain the degree of Master of Science
at the Delft University of Technology,
to be defended publicly on 31 March, 2021 at 02:00 PM.

Student number:	4157370	
Project duration:	May 13, 2020 – March 31, 2021	
Thesis supervisors:	Dr. Ir. A. Sakes	TU Delft
	Ir. E. de Kater	TU Delft
Thesis committee:	Dr. Ir. A. Sakes	TU Delft
	Ir. E. de Kater	TU Delft
	Prof. Dr. Ir. P. Breedveld	TU Delft

This thesis is confidential and cannot be made public until 31 March, 2023.

An electronic version of this thesis is available at `http://repository.tudelft.nl/`.

TU Delft

Preface

Growing up in Wageningen, with two parents who both studied in Wageningen, I was always surrounded by people who were interested in nature and knew a lot about it. But as a rebellious adolescent, I definitely did not want to study in Wageningen and study somewhere which is far away from my hometown. Luckily, my favourite subjects were Match and Physics, so I decided to study in Delft. I started studying Architecture, because I was interested in buildings and wanted to design them. However, during this study, I missed the technical aspects of designing and it was a bit too subjective for me. So, after considering different studies I decided to study Applied Physics, during which I will learn a lot about interesting phenomena of the world. This study was really hard and challenging and a bit too theoretical. Additionally, I did my minor in medicine, which led to my interest and enthusiasm for the medical world. Therefore, I decided to do a bridging programme towards the Biomechanical design. After doing different studies I finally felt that this is the right one for me. The course bio-inspired design by Paul Breedveld was my favourite, before this course I never heard of getting inspiration for technical instruments from nature. My fascination for bio-inspired technology led to choosing this graduation project. In this project, I could combine bio-inspired design with designing a medical instrument. After graduating I hope I can pursue a career that combines my technical background with my interest in the medical world.

S. Treep
Delft, March 2021

Abstract

Background:The goal of minimally invasive surgery (MIS) is to perform surgery by minimal damaging the body. Compared to traditional open surgery MIS results in faster recovery and lower mortality, and is therefore the preferred method for performing a biopsy. Natural Orifice Transluminal Endoscopic Surgery (NOTES) is a type of MIS where an instrument enters the body through a natural orifice to reach the target. During NOTES an instrument enters the body through a natural orifice to reach the target. Upon entering the body via a natural orifice, first the target area needs to be reached and second, the targeted tissue needs to be transported out of the body for further examination. Currently used instruments for NOTES are suboptimal for transport through tubular organs due to damaging the tissue. In this study, a friction-based transport mechanism, inspired by eggs of parasitic wasps, was developed as an improved tool for NOTES. Additionally, the possibility to steer this instrument was examined as well.
Methods: State of the art mechanisms were analysed and selected based on their potential for being used as a flexible system for locomotion through a tubular organ and tissue transport. Requirements of this instrument were determined which were divided into requirements for the flexible shaft and for the actuation of the locomotion and transport mechanism. Requirements were also determined for the additional wish for the instrument to be steerable. Based on these requirements a final design of a flexible shaft and actuation was developed. The design process for steerability of the flexible shaft is described as well, resulting in a tip that can be added to the flexible shaft to add steerability. Performance of the flexible shaft was evaluated based on locomotion through a tube, tissue transport and steerability in a simulated setting. The flexible shaft was tested if it is possible to locomote through a tube, transport tissue and can be steered.
Results: The developed instrument was able to locomote in a straight direction and three different configurations: with a bending radius of 80 mm, 105 mm and 130mm and a bending angle of 45°, 30° and 15 °, respectively. The locomotion rate in the straight direction was 6.17 ± 0.27 mm/cycle and was 5.21 ± 0.21 mm/cycle in the maximum bent direction (bending radius of 80 mm). The instrument was adequate for the intended use: (1) insertion into a tube, (2) locomote through the tube, and (3) transport tissue out of the tube using the flexible shaft. Adding the tip and attached steering wire ropes with manual operation allowed the shaft to be steered up to an angle of 90° with a bending radius of 58 mm.
Discussion and conclusion: A flexible shaft instrument was developed that was able to locomote and transport tissue through a tube. Additionally, a steering tip was designed that allowed to steer the instrument from outside the body/tube. While lower locomotion rates were observed for lower bending radii, the developed design shows great potential for an instrument to perform NOTES with minimal burden for the patient.

Keywords

Flexible - Friction-Based - Locomotion-Transport - Bio-inspired - Minimally invasive - Tubular organ

Contents

Glossary

Abdomen Part of the body between the thorax (chest) and pelvis.

Anisotropic When a material is anisotropic, it has different properties in different directions, which is opposed to isotropy.

Bevel tip A tip with a slope, this means that the tip is not flat but has an angled surface.

Blades The reciprocating parts that move in a certain sequence to locomote the shaft through the tubular organ and transport tissue as well. In the flexible friction-based transport each blade consists of three wire ropes and a slider.

Degrees of freedom (DoF) Number of independent values that can vary in space.

Distal Situated away from the centre of the design.

Lumen The inner space of a tubular structure. In the designs discussed it is the inner space between the inner wire ropes.

Ovipositor A tubular organ of a female wasp through which eggs are transported.

Phantom tissue Tissue mimicked by a different structure, such as gelatin.

Proximal Situated near the centre of the design.

Scale A thick, dry flake of skin.

Wire rope A number of strands of wires that are twisted around each other to form one composite rope.

1 Introduction

1.1. Background

1.1.1. Minimally invasive surgery

Minimal invasive surgery (MIS), during which the instrument is inserted through a small incision in the skin, allows reaching the target with minimal additional damage to the body. For this type of surgery an instrument is inserted through a small incision in the skin. In this way the target area can be reached. Compared to conventional open surgery, the patients recover faster and the mortality after the surgeries is lower [15]. Laparoscopic surgery is such a kind of MIS. During this surgery, a small incision is made in the skin through which an instrument is passed to enter the abdomen and pelvis. Alternatively, the instrument can be inserted through a natural orifice such as the anus or the mouth. Different instruments are required to perform MIS from different locations in the body. This study is focused on instruments used for MIS from natural orifices, designed for tissue transport. Tissue transport is important to obtain tissue that requires further examination, such as tumour tissue. Currently, tissue transport is performed by using a forceps to grasp the tissue and remove it from the body. Alternatively, the tissue can be transported by using pressure difference, where the tissue is removed via suction. Both methods have their disadvantages, the use of pressure difference is likely to damage surrounding healthy tissue/cells and using a forceps can bring damage to the transported tissue.

1.1.2. Natural Orifice Transluminal Endoscopic Surgery

Natural Orifice Transluminal Endoscopic Surgery (NOTES), is a emerging type of MIS, where the endoscope can enter the body transorally or transanally. This allows reaching areas without making an incision in the skin, such as the abdomen and the pelvis [4]. Compared to laparoscopic surgery, NOTES is less invasive, eliminates the need for an abdominal incision, causes less post-surgical pain in the abdominal wall and decreases wound infections [20]. Endoscopes exist in different designs, with different purposes. The one that is used as a reference in this study is a colonoscope, which enters the body transanally and is passed through the colon. However, this method has some disadvantages. Due to the manual control of the colonoscope the colonoscipe can hit the colon wall, especially at loopings and flexures of the colon. Since maximal forces of 29.4 N have been reported this can be very painful for the patient [5, 14, 19]. During a colonoscopy, it is also possible to remove a colon polyp, which is an abnormal growth of tissue on the inner surface of the colon. Most of these polyps are harmless but they can develop into colon cancer [16]. The polyp can be cut from the inner surface using different methods, but all methods transport the poly by using a forceps. As described above, this is suboptimal since the polyp can be damaged during the transport.

1.2. Problem definition

As stated in the previous section, the main problem during colonoscopy is the force exerted on the wall of the colon, which causes pain to the patient. This force is especially higher when the colonoscope has to move through flexures and loopings. Additionally, the method to transport a polyp out of the body is suboptimal. Therefore an instrument is needed that locomotes through the colon and follows

the curves of the colon and, when reaching the target tissue, transport the polyp/tissue out of the body without damaging it.

1.3. Ovipositor friction-based transport

1.3.1. Bio-inspired design

Friction-based transport, inspired by the transportation of the eggs of wasps, can potentially provide an optimized method for locomotion through a tubular organ such as the colon and tissue transportation. Female wasps are able to transport their eggs and lay them in different kind of materials. They lay their eggs in a host which provides nutrition for the eggs, such as a piece of fruit or a leaf and tree bark [3, 9]. Female wasps lay their eggs using the ovipositor, a tube-like organ. As can be seen in Figure 1.1 the ovipositor consists of four segments, which are called valves. Since the two top valves are merged, the ovipositor consists of three valves that slide along each other. The two merged valves constitute the largest valve, located at the top of the ovipositor called the dorsal valve. The valves will stay in the same radial position due to a tongue-and-groove mechanism [18]. The dorsal valve has small appendages, the 'tongue', and the bottom valves (ventral valves) have grooves which are shown in Figure 1.1. Together these valves envelop a duct: the oviduct, through which the eggs are transported [3]. It is hypothesized that the eggs are transported due to the rough surface of the oviduct. This rough surface creates friction between the eggs and the wall and due to the back and forward movement of the valves the eggs are transported. While the exact motion sequence of the valves is unknown, it it

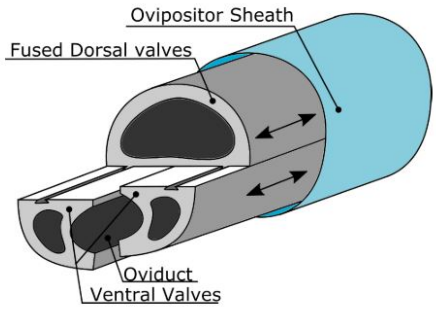

Figure 1.1: The ovipositor of a wasp including the three valves: the two ventral valve and merged dorsal valves. These valves surround the oviduct and are covered by a ovipositor sheath. The valves move back and forth, which is indicated with the arrows, to transport the eggs through the oviduct[10].

hypothesized to start with simultaneous movement of the valves in the distal direction to make contact with the egg, shown in Figure 1.2. The egg in the ovipositor will then move in the distal direction as well due to the friction between the valves and the egg, shown in the second image in Figure 1.2. When the valves are in their most distal position, they will move back to the most proximal position. This is executed one by one, shown in the third, fourth and fifth image in Figure 1.2 [10]. It is hypothesized that the oviduct is covered by scales that are orientated in such a way that that only allows forward motion of the eggs due to anisotropic friction [3, 10]. During the one by one retraction of the valves, the two stationary valves keep the egg in place while the other valve moves proximal, shown in Figure 1.23. This motion cycle of the valves, shown in Figure 1.2 is repeated until the egg reached its destination, the tip of the ovipositor.

1.3.2. Prior work: Self propelling ovipositor friction-based transport

In the design of P. Posthoorn [17] a propulsion mechanism is developed which is inspired by the ovipositor friction-based transport of the wasp. These valves of the mechanism will from now on be addressed as blades. As the valves are components of the friction-based transport of the wasp and blades are the components in the friction-based transport mechanisms designed by a human. The movement of the three valves, explained in the previous section, is translated and optimized into an algorithm that is responsible for the propulsion of six blades. This propulsion algorithm is shown in Figure 1.3 B. In each state, one blade moves forward with respect to the other blades and slides along the surface of the lumen. During this sliding, the frame of the device moves also forward [17]. The

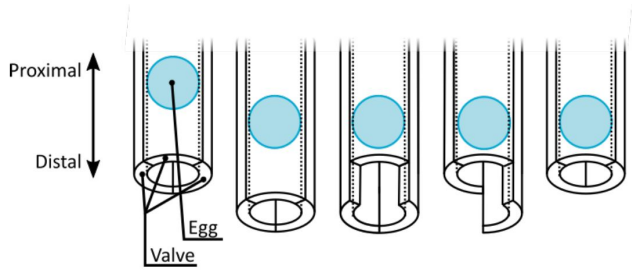

Figure 1.2: The different steps of the motion sequence of the valves to transport the egg. The first image shows the egg at its start position surrounded by the valves. In the second image, all the valves move distal which caused the egg to transport more distal as well due to friction. In the third and fourth image, these valves move proximal one by one. In the fifth image, all these valves are moved proximal and the steps can be repeated [10].

different positions of these blades are shown in Figure 1.3 A. The black line shows how they move from one state to the other. All the blades move along this path but with a delay relative to each other. The positions of the blades are controlled by attaching each blade to a pin that follows the path that is created on the outer surface of a cylinder, called a barrel cam and shown in Figure 1.3 C.

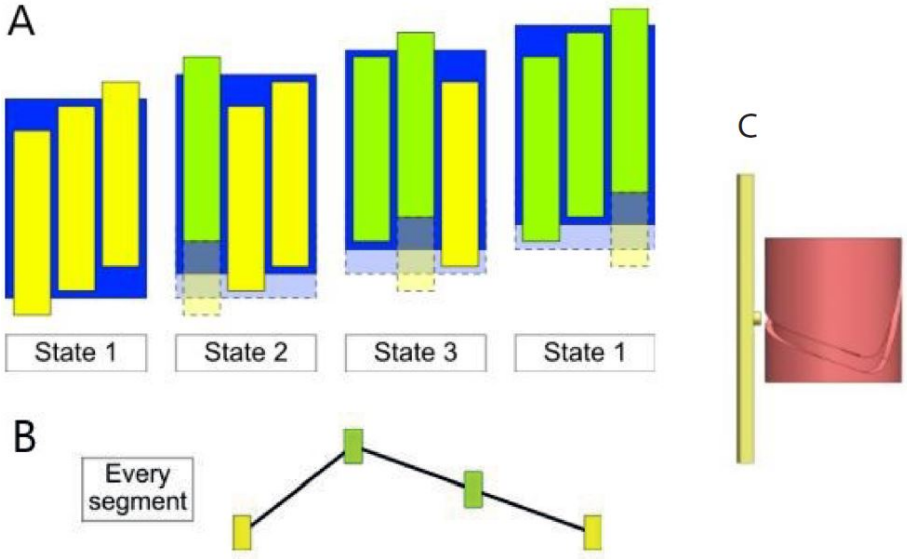

Figure 1.3: (A) Schematic representation of the optimized propulsion algorithm. The yellow and green rectangles represent blades that can move back and forth individually. The blue rectangle is the frame of the device. During all these different states one blade moves forward with respect to the other blades. This means it will slide along the wall of the lumen at the same time the frame moves forward as well with respect to the stationary blades and the surroundings [17]. (B) The path each blade will follow when moving from one state to another. Between the blades, a time delay is present [17]. (C) A barrel cam (shown in red) will be rotated. As the pin of the blade (shown in yellow) is placed on the path, the blade will move back and forth due to the rotation of the barrel cam [17].

1.3.3. Prior work: Endo-Tubular Friction Carrier

A number of designs are inspired by the friction-based transport of eggs along the ovipositor. One of these designs is the endo-tubular friction carrier of I. van der Steeg. He designed a rigid transport system that consists of six blades instead of three valves, shown in Figure 1.4.

In his final concept, the motion of the tissue is created by the friction between the surface of the six semi-circular blades and the tissue. In a stylized situation, the tissue is transported with the combined friction of the six blades. All these blades contribute equally to the total friction, each supplying one-sixth of the total friction. Consequently, the friction of five blades will outweigh the friction of one blade, and the friction of four blades will outweigh the friction of two blades. In other words, the friction of the majority of the blades will always exceed the friction of the minority [24]. Therefore, the tissue can be

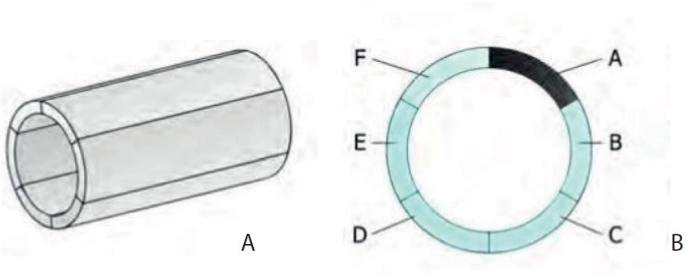

Figure 1.4: (A) The endo-tubular friction carrier consisting of six blades [24]. (B) Numbering of the six blades. One of them, A (displayed in black), will move forward while the others, shown in blue, move gradually backwards [24].

transported unidirectionally by ensuring that at any point in time, a majority of the blades move in the desired transport direction.

Based on this principle, two different motion sequences for tissue transport were developed. The first one is the hexasected reciprocating sequence. It is called hexasected, because the transport system consists of six parts: the blades. In Figure 1.4 the six blades of this sequence are shown. One blade is represented in black and the others in blue. The blades will move back and forth in such a way that five blades move forward while one blade moves backwards. This causes the tissue to move forwards as the friction between the tissue and the five blades is larger than the friction between the tissue and one blade. The exact motion sequence steps and extensive explanation can be found in Appendix A. A second sequence, which consist of three groups of opposing blades and therefore called the trisected reciprocating sequence, was found to be less successful in tissue transport. Therefore, this sequence is not further discussed in this report.

1.3.4. Prior work: Flexible friction-based transport system

The Endo-Tubular Friction Carrier [24] was further developed by E. de Kater with the main aim to make the design more compliant. The rigid blades of the Endo-Tubular Friction Carrier [24] were replaced by blades consisting of wire ropes to make the flexible shaft even more flexible, allowing movement in any direction of the plane of the shaft. The wire ropes were held together by magnetic rings, and since the wire ropes are made out of galvanised steel they will be attracted by the magnetic rings. Compression springs are placed between the magnets to keep the magnets in place without restricting the shafts flexibility. Around the wire ropes, magnets and springs, a heat shrinking tube is placed to prevent the transported tissue to escape from the flexible shaft. In Figure 1.5 this configuration is shown.

The wire ropes, shown in red in Figure 1.5 have the same working principle to transport the tissue as the semi-circular blades of the Endo-Tubular Friction Carrier [24]. Instead of six blades, the tissue is now transported by eighteen wire ropes with a diameter of 0.6 mm, shown in Figure 1.6. The eighteen wire ropes are clustered into six groups of three wire ropes, to replace each rigid blade with a flexible blade consisting of three wire ropes. The flexible blades are actuated in the same way as the blades of the Endo-Tubular Friction Carrier [24].

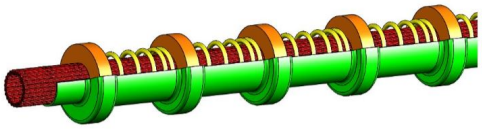

Figure 1.5: The design of the flexible friction-based transport system. The wire ropes (red) form a lumen by the magnetic force between them and the ring magnet (orange). Between the magnets, compression springs are present (yellow). All these components are covered by a heat shrinking tube (green) [10].

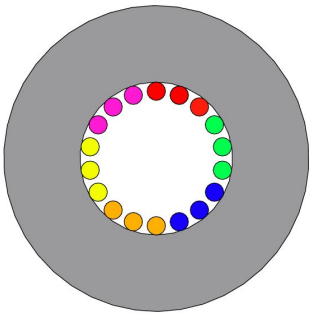

Figure 1.6: A schematic view of the wire ropes, grouped into six blades. Each blade consist of three wire ropes, displayed in the same colour. The grey ring around the wire ropes represents the ring magnet.

1.4. Goal of the study

The goal of this study is to design, manufacture and test a double-walled friction-based locomotion and transport mechanism. This double-walled design combines tissue transport and locomotion and the possibility to steer is explored as well. This design will be bio-inspired, as it is inspired by the ovipositor of the wasp. This designed mechanism consists of two rings (walls). The inner ring will be responsible for the transport of the tissue and the outer ring for the locomotion of the flexible shaft. The design will be tested if it is able to locomote through a tube and transport the tissue from the target area and if it is possible to be steered into the desired direction.

1.5. Layout of the report

In Chapter 2 the design process of the instrument will be described. The final design of the flexible shaft including all its component is described in Chapter 3. How the locomotion and tissue transport are actuated is illustrated in Chapter4. The optional characteristic of the flexible shaft: steerability is discussed in Chapter 5. The validation experiments are illustrated in Chapter 6. These experiments led to results which are shown in Chapter 7. In Chapter 8 these results are discussed and improvements for the design are suggested. In Chapter 9 a conclusion is drawn. At the end of this report is an Appendix with more background information and the technical drawings of the prototype.

2

Design process

2.1. Proposed solution

The proposed solution design consists of a flexible shaft encompassed of two rings. The inner ring (displayed in red) in Figure 2.1 will be responsible for the tissue transport and the outer ring (displayed in green) in Figure 2.1 will be responsible for the locomotion of the flexible shaft and the steering. Consequently, this flexible shaft combines the transport of the tissue with locomotion through the tissue to reach the tissue it has to transport. The flexible shaft needs to be easy to use, by the hand of the user.

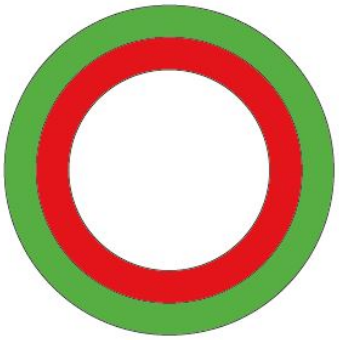

Figure 2.1: A section view of the flexible shaft. The shaft consist of two rings: the inner ring (red) and outer ring (green). The inner will be responsible for tissue transport and the outer ring for the locomotion of the shaft.

Below, the intended use of using the flexible shaft is described, which is also shown in Figure 2.2.

1. Insert the flexible shaft into the tubular organ
2. Move to the target by the locomotion of the outer wire ropes
3. (Optional) Change the path of the locomotion by steering of the shaft
4. Transport tissue by the inner wire ropes

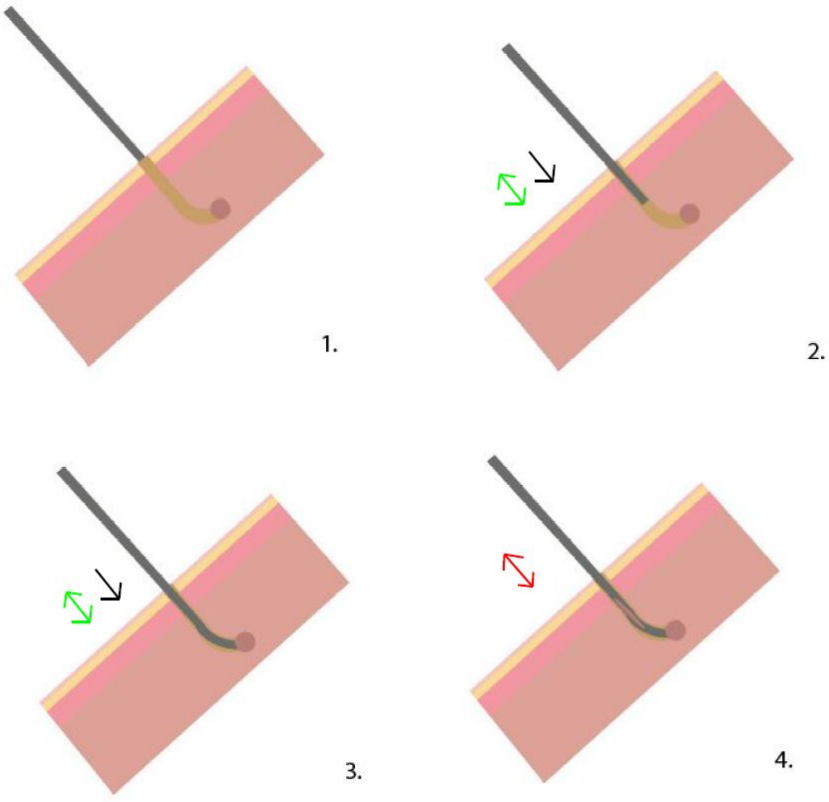

Figure 2.2: Intended use of the procedure. The black arrow indicated the movement of the flexible shaft, the green arrow indicates the movement of the outer wire ropes and the red arrow the movement of the inner wire ropes. (1) Insertion of the flexible shaft into the orifice. (2) The back and forth movement of the outer wire ropes causes the flexible shaft to locomote to the target (indicated by the brown circle) through the tubular organ. (3) Steering the flexible shaft to reach the target, this step is only possible when adding steerability to the design. (4) Transport of tissue by back and forth movement of the inner wire ropes.

2.2. Design requirements

2.2.1. Flexible shaft requirements

These requirements concern the characteristics of the flexible shaft, which will locomote through the tubular organ and transport tissue.

- **Lumen diameter** To transport the tissue, an open lumen is required. Through this lumen, the tissue will be transported. As the design of this study is an innovated version of prior work [10, 24], it was chosen to require the same diameter as in these designs. Additionally, the results of the tissue transport can be compared to the results of these studies. This means the lumen diameter has to be 0.4 mm. The tissue will be transported due to the friction between the tissue and the wire ropes, therefore, the lumen diameter has to be constant over the entire length of the flexible shaft.
- **Outer diameter** The instrument will be used to locomote through a tubular organ. The outer diameter of the instrument depends on the diameter of this tubular organ. This could be a colon for example. An adult European human has a colon with a diameter between 23 and 36 mm [25]. However, the design will be a proof-of-concept design that will show that locomotion through a tubular organ is possible, instead of specifically through a colon. The outer diameter of prior work [10] is 10.5 mm. Therefore, it was decided to require an outer diameter of 11 mm.
- **Connection between rings** The design will consist of two rings, the inner ring is responsible for tissue transport and the outer for locomotion. These rings need to be connected; to locomote the complete shaft to the target, because the inner ring needs to transport the tissue when the target is reached. During the locomotion and tissue transport, the connection between the rings

will keep them together to ensure that not any part of the design will loose and will be left in the tubular organ.

- **Bending radius** The flexible shaft needs to follow the natural curves of the organic tubular structures of the body. A colonoscope is able to bend with a bending radius of 60-90 mm [11]. Therefore, the bending radius of the flexible shaft needs to be 90 mm. This means that the design can locomote through a tube that has a curvature with this bending radius.
- **Continuous transport of the tissue** The flexible shaft needs to transport the tissue from the tip of the flexible shaft to the end of it continuously. This means that the tissue will not be obstructed during this transport and can be taken out at the backside of the flexible shaft. To make continuously transport possible, the shaft needs to be in a straight configuration as well.

2.2.2. Actuation requirements

These requirements concern the requirements for the actuation of the flexible shaft. How the tissue transport and the locomotion of the flexible shaft will be actuated.

- **Manual actuation** The focus of the design discussed in this report is the transport of the tissue and the locomotion of the flexible shaft that is only possible when the wire ropes of the flexible shaft are actuated. This can be done in different ways, but it needs to be actuated in an easy convenient way by a human, as the focus is not on designing an innovative actuation system.
- **Two separate systems for tissue transport and locomotion** The final design will consist of two rings of wire ropes; one responsible for tissue transport and the other for locomotion. Those two rings have to be actuated separately, since the design first needs to locomote to the target where is subsequently transport the tissue out of the body.

2.2.3. Steerability requirements

The steerability of the flexible shaft is also explored in this study. The steerability requirements regards the demands for the flexible shaft when steerability is added to the shaft.

- **Bending angle** Commercialized instruments in the field of laparoscopy, usually are able to bend with an angle of ±60°, such as the Laparoflex (DEAM, Amsterdam, the Netherlands). Prior works show a device that was able to create a bending angle of 90° [10]. Therefore, the demand for the bending angle is set at 90°.
- **Bending radius** To obtain a bending angle of 90° the flexible shaft needs to be bend with a certain radius. The flexible shaft is an innovated design of the flexible friction-based transport system [10], therefore, it was chosen to set the demand for the bending radius at a maximum of 60 mm, since this mechanism obtained a bending angle of 90° with a bending radius of 59 mm.
- **Tip** The tip of the flexible shaft needs to have 2 Degrees of Freedom (DoF) to steer in the desired direction. In this way, it would be possible to change the direction of the shaft when the target cannot be reached in a straight direction and the shaft needs to follow the tubular organ.

3

Design flexible shaft

3.1. Concepts double-walled construction

As discussed in Chapter 2, the inner ring of the transport mechanism will transport the tissue and the outer ring will locomote through a tubular organ. These two rings need to be connected, together they form the shaft of the instrument. As the shaft needs to be flexible, the inner and outer ring will consist of wire ropes, since the flexible friction-based transport system [10] showed the potential of tissue transport by wire ropes. To maintain the circular shape of the inner and outer ring, a circular construction to maintain this shape needs to be positioned between these rings. The inner wire ropes will be attached to this construction to maintain its shape. The outer wire ropes will be attached to this construction to be included in the design. The different concepts for this construction are shown in Figure 3.1. Concept A shows a ring that has clamps on each side to keep the wire ropes in their position. Concept B has a nylon thread that is weaved around the wire ropes to attach them to the ring.

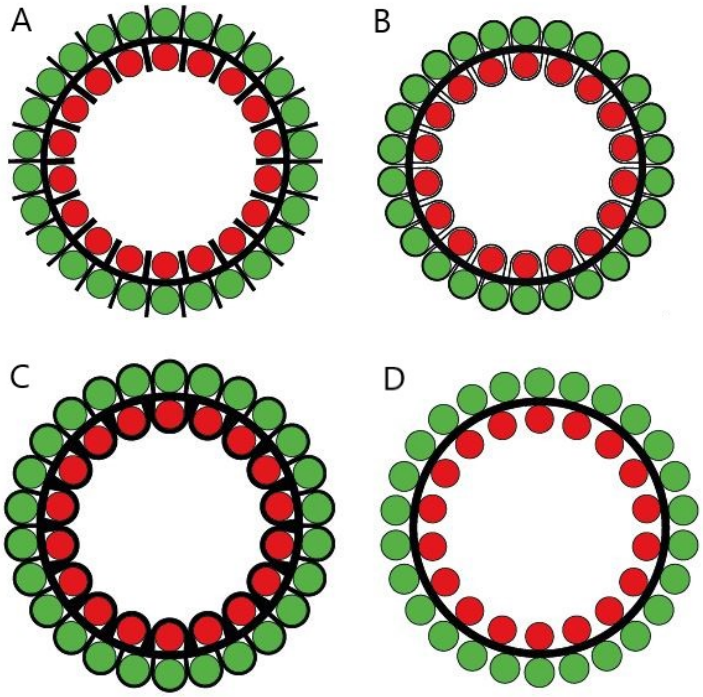

Figure 3.1: Different concepts of the construction between the inner and outer ring. (A) The positioning of wire ropes by a ring with clamps. (B) The positioning of wire ropes by a ring with weaved nylon thread. (C) The positioning of wire ropes by a weaved solid structure. (D) The positioning of wire ropes by a ring magnet.

In concept C, a developed version of concept B is shown. Instead of nylon thread, the wire ropes are weaved by a structure included in the ring design. In concept D, a ring magnet is shown which attract the wire ropes (when a material is chosen for them which is attracted by a magnet, such as steel). The main drawback of concept C is that the ring configuration covers part of the surface of the wire ropes. This will decrease the surface between the tissue and the wire ropes and the surface between the wire ropes and the surface of the tubular organ. This could negatively influence the performance of friction-based transport.

The decrease of surface between the tissue and wire ropes is also a drawback of concept B, although the surface of the nylon thread is smaller than the surface of the ring configuration in concept C. However, weaving all the wire ropes would take a lot of time and as difficult due to the small scale of the design. When the wire ropes move back forth through the clamps in concept A, they experience a lot of friction due to the clamps. This is a major drawback as it will decrease the performance of friction-based transport. Therefore, concept D shows the most potential to develop further as all these drawbacks are not present in this concept. The wire ropes will automatically be positioned in a circular shape due to the magnetic force between them and the ring magnet. A small amount of friction will be present between the ring magnet and the wire rope. The surface between the tissue and the inner wire ropes is maximum, which applies as well to the surface between the outer wire ropes and the tubular organ.

3.2. Final Design

3.2.1. Compression springs, ring magnets and inner wire ropes

In the flexible friction-based transport system, ring magnets are used around the wire ropes to keep them in position. In this way, a lumen will be present through which the tissue can be transported. To be in this configuration, the wire ropes need to be made of a material that is attracted by the ring magnet. Therefore, galvanised steel wire ropes were chosen as this material is attracted to the magnet and was easy to obtain. The wire ropes have a diameter of 0.6 mm and eighteen of them are used, which resulted in six blades. The ring magnet will have the same size as the ones used in the flexible friction-based transport system. The magnets have an inner diameter of 5 mm, an outer diameter of 10 mm and a height of 2 mm. Between the ring magnets, compression springs will be positioned, allowing the flexible shaft to bend. These compression springs also keep the wire ropes in a straight configuration between the ring magnets, shown in a schematic image in Figure 3.2.

If the direction of the flexible shaft is changed, it is preferable to deflect the tip with a higher deflection compared to the rest of the flexible shaft. Since when deflecting the flexible shaft, the tip will need to deflect with a higher angle than the rest of the shaft. Therefore, the spring stiffness will decrease when the position of the spring is closer to the tip. The stiffness of the spring depends on its spring rate $k[N/mm]$. The higher the spring rate the more force is needed to compress the spring. Therefore, the spring rate will gradually decrease when the position of the spring is closer to the tip. Two concentric springs will be placed between the magnets, the spring with the lowest diameter will keep the inner wire ropes at their position. And the outer spring will create tension on the outer wire ropes. The position of these springs is shown in Figure 3.3 A.

3.2.2. Outer wire ropes

The wire ropes on the outside, called the outer ring, are responsible for the locomotion of the flexible shaft. Three of these wire ropes will be grouped to form one blade. Since the outer wire ropes are positioned around the magnet instead of inside the magnet they will occupy a larger diameter. Between these blades, extra space must remain available for the steering wire ropes. Since one blade consists of three wire ropes, the amount of wire ropes that will be positioned around the magnet has to be

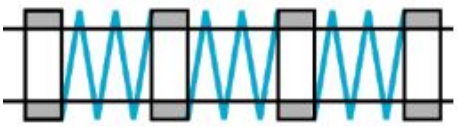

Figure 3.2: Schematic view of ring magnets (grey) and compression springs (blue) [10].

a multiple of three. The available diameter of galvanised wire ropes that could be ordered from the company Engelmann are 0.6 mm, 0.8 mm, 1.25 mm, 1.50 mm. It was calculated which diameter and how many blades are the most optimum to use and that calculation can be found in Appendix B.1. This resulted in using wire ropes with a diameter of 0.8 mm and twelve blades, which means that in total thirty-six outer wire ropes are placed around the magnets and compressing springs, shown in Figure 3.3 B. This configuration of the blades is shown in Figure 3.4. The twelve blades will be actuated in the same way as the inner wire ropes. However, the number of blades is double the number of blades of the inner wire ropes. This means that when one group is actuated, the complement group will be actuated as well. This is shown in Figure 3.4. In the final design, the compression spring with the smallest diameter was removed, since it was hard to bend the flexible shaft with these present. Also, the inner wire ropes still had enough tension to be attracted to the ring magnet to surround the open lumen. A section view of the design is shown in Figure 3.5 and in Figure 3.6 an exploded view. The prototype of the flexible shaft is shown in Figure 3.7. In Table 3.1 all these components are illustrated and described how they are connected.

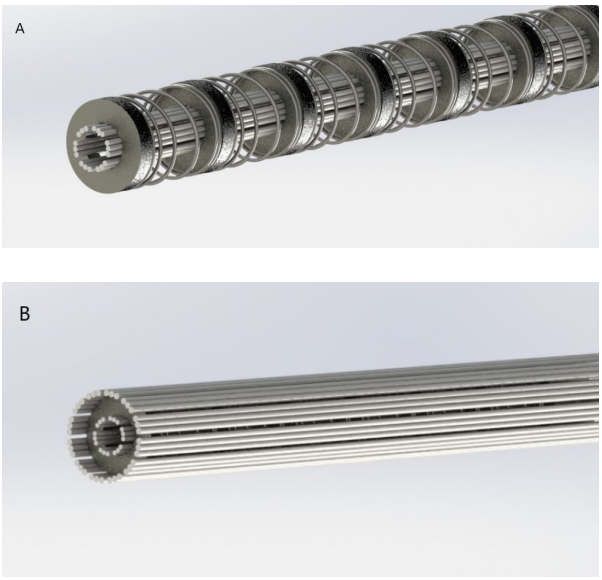

Figure 3.3: (A) An isometric projection of the components of the flexible shaft, except the outer wire ropes. The inner wire ropes form an open lumen due to the magnetic force of the magnetic rings around them. Between all the ring magnets two concentric compression spring are positioned. (B) An isometric projection of the flexible shaft, which shows the inner wire ropes and the outer wire ropes.

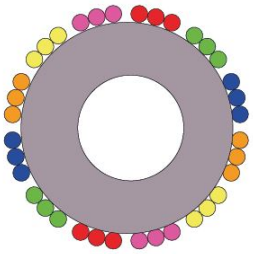

Figure 3.4: The outer wire ropes are grouped in six groups, indicated with the colors: red, green, blue, orange, yellow and pink. The wire ropes with the same color form one blade and are actuated at the same time.

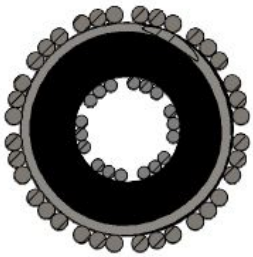

Figure 3.5: A section view of the flexible shaft. The inner wires are shown in dark grey, the outer wires in light grey. The black area of the circle presents the ring magnet and the grey outer circle the compression spring.

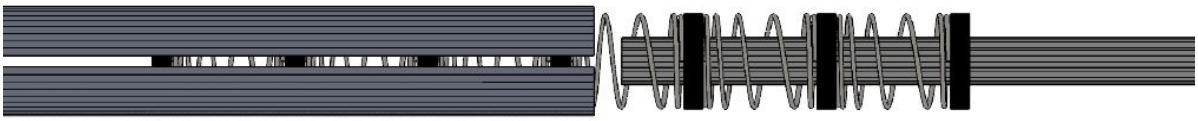

Figure 3.6: Exploded view of flexible shaft. From left to right: the outer wire ropes, the magnets and compression spring, the inner wire ropes.

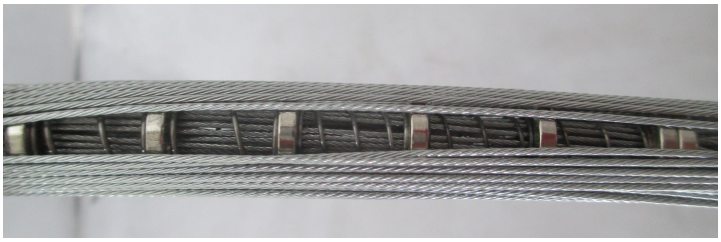

Figure 3.7: The prototype of the flexible shaft, which includes the inner and outer wire ropes, ring magnet and compression springs.

Table 3.1: Overview of the components of the flexible shaft with detailed information and their connection to each other. With d = diameter, di=inner diameter, do=outer diameter, h=height, l=length, pf=spring rate.

Component	**Details**	**Production method/ Acquisition details**	**Amount**	**Connection**
1. Inner wire ropes	galvanished steel d = 0.6 mm	Bought: Engelmann	18	Connected to the magnets (2) by magnetic force
2. Ring magnet	neodynium di = 5 mm do = 10 mm h = 2 mm	Bought:Conrad	4	Connected to the wire ropes (1,4), and to spring (3) by magnetic force
3. Compression springs	steel do = 9.14 mm pf = 0.51 N/mm, 0.77 N/mm, 1.12 N/mm 1.61 N/mm, 2.26 N/mm and 3.13 N/mm l=12.7 mm	Bought: Amatec	6	Connected to the magnets (2) by magnetic force
4. Outer wire ropes	galvanished steel d = 0.8 mm	Bought: Engelmann	36	Connected to the magnets (2) by magnetic force

4

Design actuation

4.1. Concepts cams and handle

To actuate the three characteristics of the design, locomotion, transport and steerability, a prototype needs to be manufactured. This prototype will consist of two cams, which will be responsible for the translation of the transport of the wire ropes. The original design of the cam, the barrel cam, has the path on the outer surface, which is shown in Figure 4.1 A. However, this does not allow for continuous transport of the tissue, as the cam then obstruct the open lumen. Therefore, in the flexible friction-based mechanism [10] the barrel cam was changed to an inside-out cam, which is shown in Figure 4.1 B. The inner cam needs to be an inside-out cam to allow continuous transport of the tissue. A handle for the steering wire ropes needs to be included as well, because then it is possible to add steerability to the design. This handle is attached to the steering wire ropes and when rotated it will steer the flexible shaft in the desired direction. The possible concepts of the positions of the cams and handle are shown in Figure 4.2. They all can be placed at a different position, but the cams can also be placed in the same plane. This is not possible with the actuation of the steering wire ropes as the handle needs freedom in space to bend in the desired direction. It is also inconvenient to position the handle between the cams, as the cams have to be connected to the ground and the handle needs movement space.

In concepts A and B the cams are both situated distal to the handle and in a different plane. In concepts C and D the cams are placed proximal to the handle and in a different plane. The two last concepts E and F differ from these concepts, as in these concepts the cams are positioned in the same plane. When these cams are placed in another plane, it would be more difficult to actuate these cams with a sling connected to the cam, as the sling of the cam more proximal cannot be reached. However, this can be solved by enlarging the thickness of the most proximal cam. It was chosen to place the cams in the same plane, which makes it more convenient for the user to actuate them. Also positioning the handle distal to the plane of the cams will be a more logical concept than positioning it proximally, since when the handle is at the most distal position the user has the most room for movement. When the cams are positioned in the same plane, two different concepts are possible for the cam: the barrel cam and the inside-out cam. The outer cam could be a barrel cam or an inside-out cam. Those two

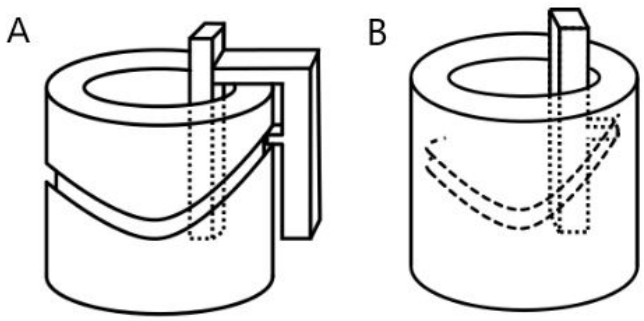

Figure 4.1: (A) Barrel cam (B) Inside-out cam [10].

concepts are shown in Figure 4.3. The barrel cam has the problem that when one of the two cams rotates, friction will decrease the rotation velocity. Since the surfaces of the inner and outer cam touch each other. This could be solved by creating more space between them or place a ball bearing between them. The outer wire ropes are less supported when the outer cam is a barrel cam as well, as they are only connected to the sliders. The outer wire ropes will be more supported when the outer cam is an inside-out cam, which is shown in Figure 4.3 B. However, friction between the inner cam and the outer inside-out cam will decrease the rotation velocity. However, the main issue of the outer barrel cam is that it is less convenient to rotate one cam, since they are positioned close to each other. As one of the requirements is that it is convenient to rotate just one cam, it was chosen to develop the concept with the inside-out cam as outside cam, shown in Figure 4.3 A.

4.2. Final design

4.2.1. Tissue transport components

The inner sliders are connected to the wire ropes responsible for tissue transport. Each slider is glued to three wire ropes, together this is one blade. This makes up a total of six blades, which will follow the path inside the inner cam, shown in Figure 4.5. The blades will follow the path of the cam, as the pin of the slider, shown in Figure 4.4, will be placed into the path. Since the pin of the slider needs to easily follow the path, the angles of the path: α and β needs to be small. Therefore, the demand for the width of the right part of the path, shown in Figure 4.5, is that it has to be equal or smaller than $\frac{1}{n} * 2\pi * R_c$. In which n represents the number of blades and R_c the radius of the cam. The inner cam is shown in Figure 4.6 A. Due to the rotation of the inner cam, the slider will follow the path of the cam, shown in Figure 4.5. The rotation of the cam is done by rotating a sling that is attached to the cam. The sliders translate the rotational movement of the cam into the linear movement of the wire ropes. The stroke length, indicated in Figure 4.5, is the distance the shaft will locomote by one rotation of the cam. This length is set to 5 mm, as this was the set length as well in prior work [10, 24].

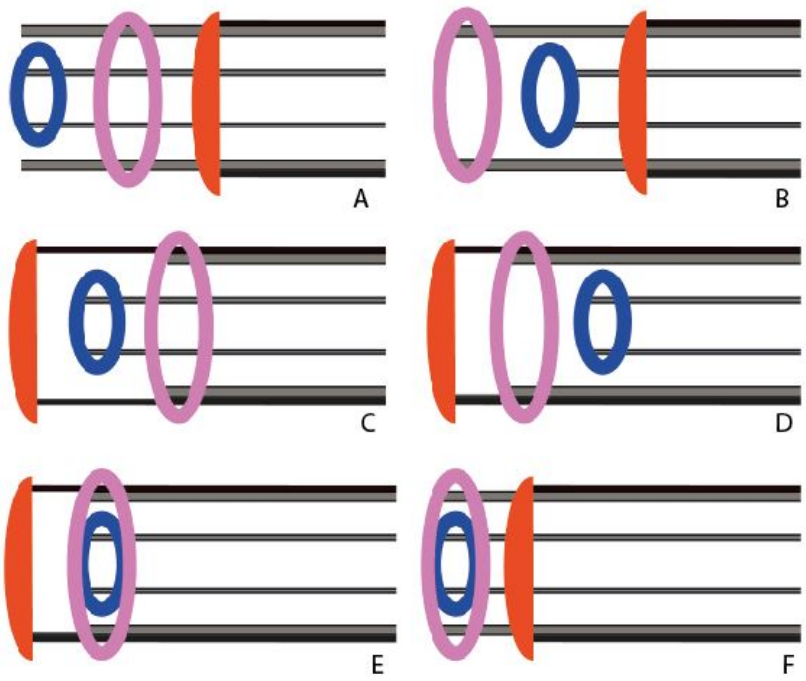

Figure 4.2: The six concepts for positions of the inner cam (blue), outer cam (pink) and handle (red) relative to each other. The inner and outer wire ropes are displayed in grey and the steering wire ropes in black. The cams and handle are positioned on the left side of the shaft.

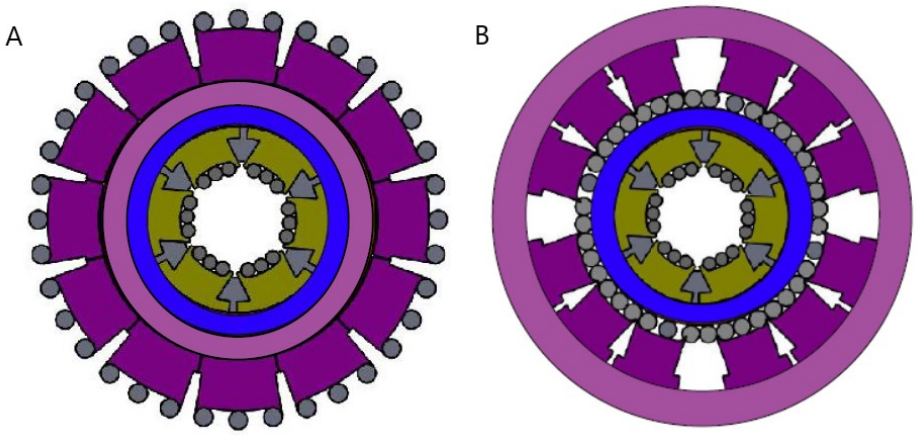

Figure 4.3: (A) The outer cam (pink) which has the path on the outside, just as the barrel cam. The outer sliders are displayed in purple and attached to the outer wire ropes (grey circles). The inner cable wire ropes are shown in grey circles as well and attached to the inner sliders (yellow). The inner cam is shown in blue. (B) The outer cam (pink) has the path on the inside, just as the inside-out cam. The outer sliders (purple) are attached to the outer wire ropes (grey circles). The inner cable wire ropes (grey circles) are attached to the inner sliders (yellow) as well. The inner cam is shown in blue.

4.2.2. Locomotion components

The outer sliders are connected to the wire ropes which are responsible for the locomotion of the flexible shaft. Each slider is glued to three wire ropes and together they are one blade. In total there are twelve sliders, which will follow the path inside the outer cam, shown in Figure 4.6 A. As these sliders are double the amount of the sliders used for tissue transport, the path of the cam, shown in Figure 4.6 B has to be doubled in the circumstance of the cam. This means that the length of one path needs to be $\frac{2*\pi*R_c}{2} = \pi * R_c$. The stroke length is set to 5 mm, which is the same as the stroke length of the tissue transport.

As the outer wire ropes are positioned in a circle with a large diameter, shown in Figure 4.8, it was possible to still meet the requirements of the right part of the path, shown in Figure 4.5. This means that the right part is equal to $\frac{1}{6} * 2\pi * R_c$, since the amount of sliders in one path is six. In total twelve sliders are present in the doubled path of the outer cam. This means that complement blades are actuated at the same time, these complement blades are shown in Figure 3.4.

4.2.3. Supporting actuation components

The two cams need to be supported to keep at their position and the outer wire ropes need a structure that dilates them. This structure is the inner cone, shown in light blue in Figure 4.7 and Figure 4.8. This inner cone consists of a house, which keeps the inner sliders (shown in yellow) at their position. The outer part of this cone is the exterior with grooves for the outer wire ropes. This part is responsible for the dilation of the locomotion wire ropes. In this way, the outer sliders (shown in orange) will be

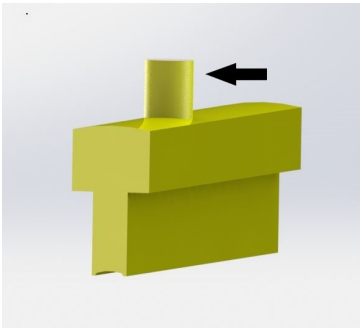

Figure 4.4: The inner slider. The pin of this slider, indicated with the arrow, will follow the path of the cam and therefore will translate rotational movement into linear movement.

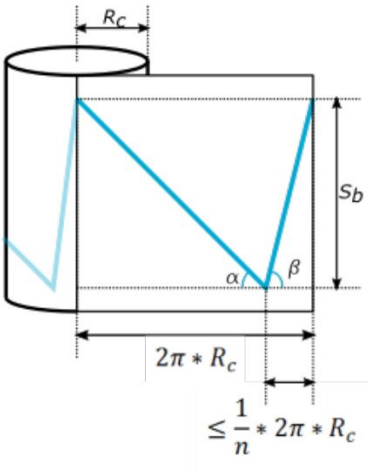

Figure 4.5: The path which the slider follows shown by the blue line. R_c represents the radius of the cam, $2\pi * R_c$ represents the circumstances of the cam. And S_b the stroke length. The width of right part of the path has to be smaller than $\frac{1}{n} * 2\pi * R_c$, in which n is the number of blades. α and β represents the angles of the path. [10].

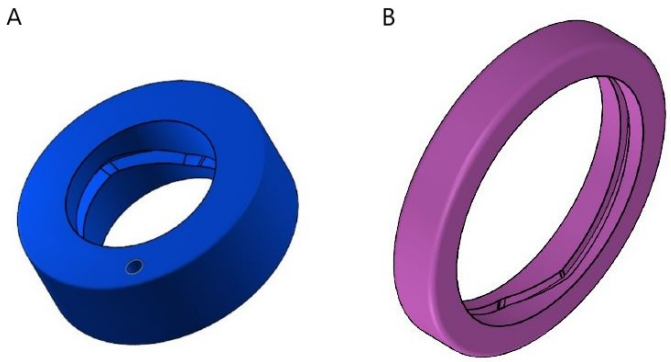

Figure 4.6: (A) The inner cam. The inner sliders will follow the path on the inner surface of the cam when the cam is rotated. (B) The outer cam. The outer sliders will follow the path on the inner surface of the cam when the cam is rotated.

positioned on a larger diameter, than the inner sliders. The slider house (shown in green), will keep the outer sliders at their position. The outer cone (shown in purple), will keep the locomotion wire ropes in position and make it possible to place the complete actuation system into a holder. How these components are connected can be found in Table 4.1. A front view of the actuation design is shown in Figure 4.9 and a side view is provided in Figure 4.10 In Figure 4.11 a front view of the prototype is shown and a side view is provided in Figure 4.12

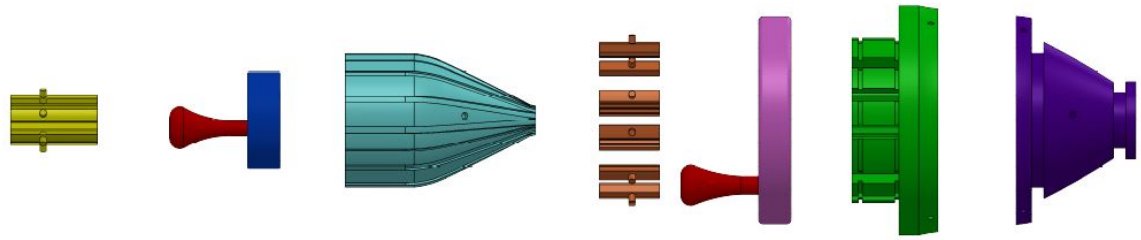

Figure 4.7: Exploded view of the actuation design. The inner sliders (yellow) are connected to the inner cam (blue) which is already screwed to the sling (red). These components are placed in the inner cone (light blue). Then the outer sliders (orange) are connected to the outer cam (pink) which is already screwed to the sling (red). The outer cam and sliders are placed around the slider house (green) and placed around the cone, inner cam and inner sliders. The outer cone (purple) is placed around the inner cone and screwed to the inner cone (light blue) and slider house (green).

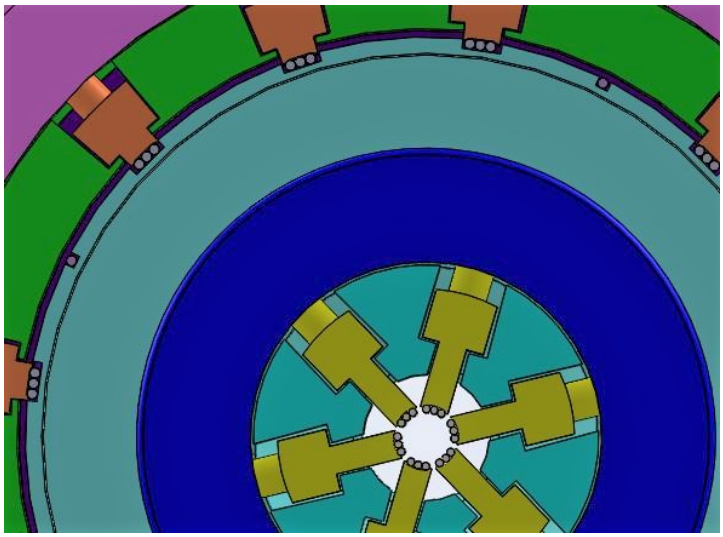

Figure 4.8: A zoomed in front view of the actuation design. The inner sliders (yellow), placed in the inner cone (light blue) with the glued wire ropes (grey circles). The outer sliders (orange) are positioned around the inner cone (light blue) cone with the glued wire ropes (grey circles).

Table 4.1: Overview of the components of the flexible shaft with detailed information and their connection to each other.

Component	**Details**	**Production method/ Acquisition details**	**Amount**	**Connection**
1. Inner slider	See Appendix E	Electrical discharge machining	6	Connected to inner wire ropes by glue
2. Inner cam	See Appendix E	3D-printing	1	
3. Inner cone	See Appendix E	3D-printing	1	Connected to outer cone (7) by screws
4. Outer sliders	See Appendix E	Electrical discharge machining	12	Connected to outer wire ropes by glue
5. Outer cam	See Appendix E	3D-printing	1	
6. Slider house	See Appendix E	3D- printing	1	Connected to outer cone (7) by screws
7. Outer cone	See Appendix E	3D-printing	1	Connected to inner cone (3) and slider house (6) by screws
8. Sling inner cam	See Appendix E	3D printing	1	Connected to outer cam (5) by screw
9. Sling outer cam	See Appendix E	3D printing	1	Connected to outer cam (5) by screw

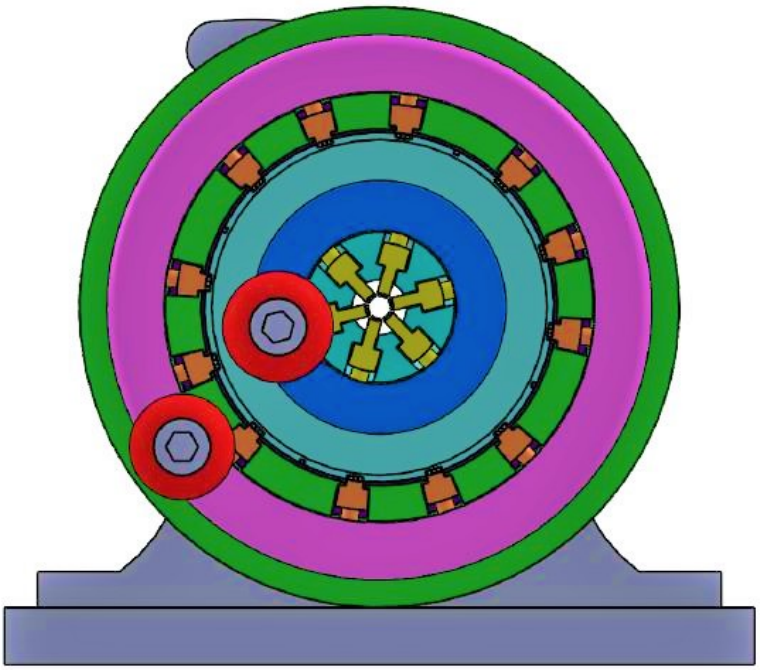

Figure 4.9: Front view of the actuation design. The grey components the holder in which the actuation design is placed. The following components are shown: outer cam (pink), slider house (green), inner cone (light blue), inner cam (light blue), inner sliders (yellow), slings (red).

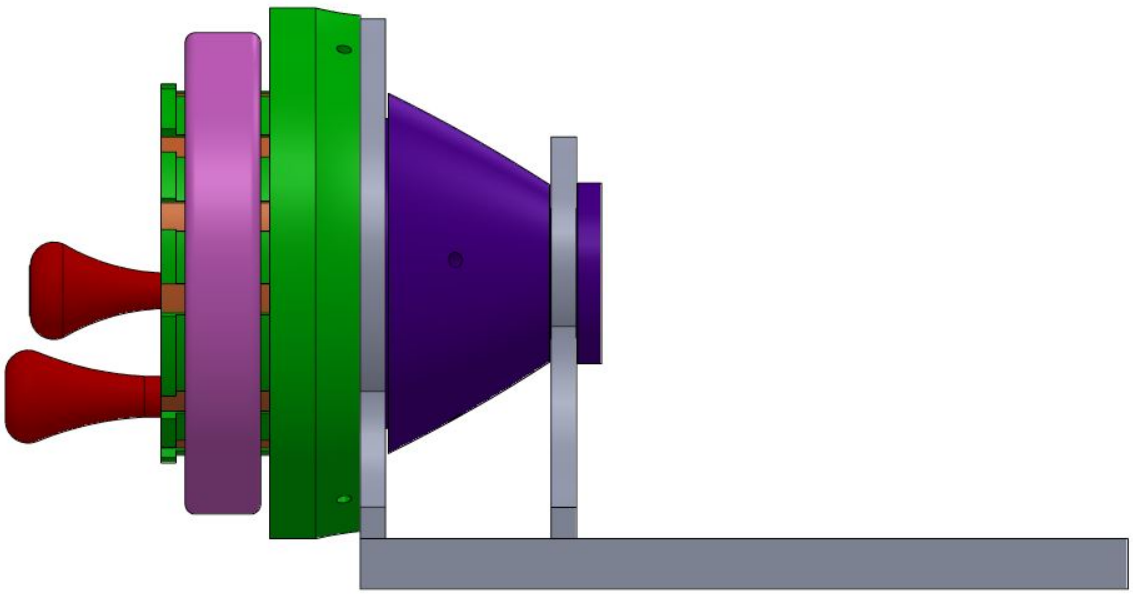

Figure 4.10: Side view of the actuation design. Grey represents the holder in which the actuation design is placed. The following components are shown: outer cam (pink), slider house (green), slings (red), outer cone (purple).

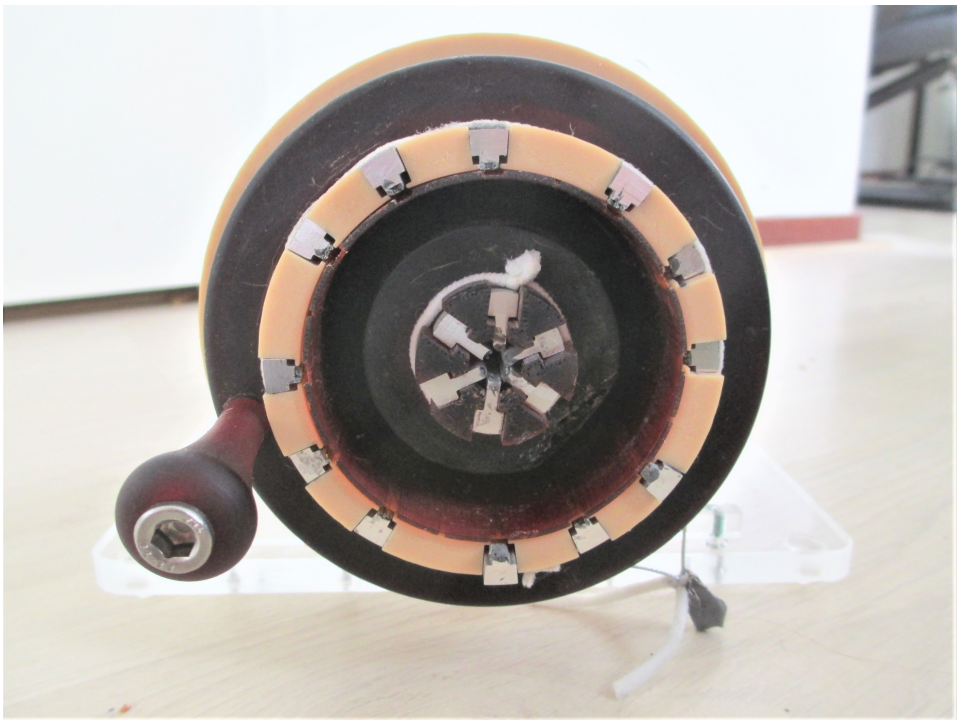

Figure 4.11: Front view of the actuation part of the prototype.

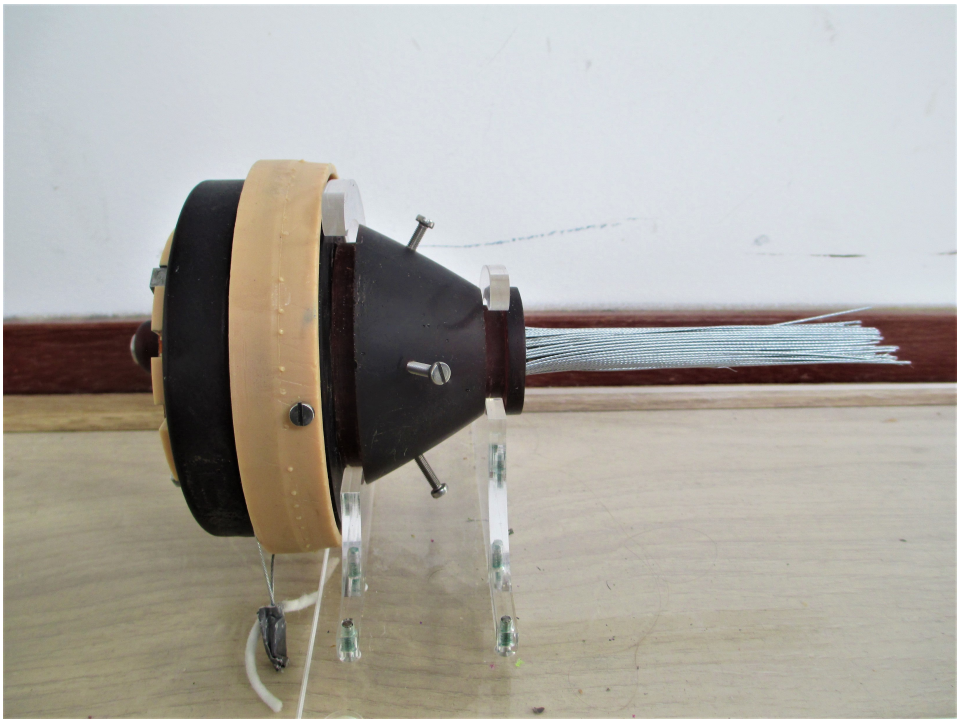

Figure 4.12: Side view of the actuation part of the prototype including the flexible shaft.

5

Adding steerability to the prototype

5.1. Concepts of steerable tip

The possibility to steer the flexible shaft was also explored. First, a categorization was done of different methods to steer a device, which can be found in Appendix C.1. Which lead to the result that a user-defined device is the best option. Since a user-defined device can be adjusted by the user actively to steer in the desired direction. Three user-defined devices were compared to each other, a description and comparison of those three designs can be found in Appendix C.2. This led to concepts that are a combination of two of the user-defined devices. The concepts all include four steering wire ropes, this mechanism was used in the design of N. van de Berg [23] and shown in Figure 5.1 A. These four steering wire ropes makes it possible to steer the flexible shaft in 2 DoF. In the design of P. Breedveld [7], the flexible endoscope consisted of a ring of wire ropes which were squeezed between a tip, to keep the wire ropes at their position at the tip of the endoscope. This is shown in Figure 5.1 B. This combination of the steering wire ropes and the tip is fundamental for all the concept to add steerability to the flexible shaft.

It was chosen to include the steering wire ropes in the outer ring of wire ropes wires and not in the inner ring. In this way, a lower force is needed to steer, as due to a larger distance vector a higher bending moment is achieved with the same force. In Figure 5.2 the concept is shown for the steering wire ropes. The four steering wire ropes will be attached to a tip and all other wire ropes in this ring will be responsible for the locomotion of the flexible shaft. The tip can be attached to the steering wire ropes in different ways. Different solutions are shown in Figure 5.3. The basic principle of all these concepts is creating a ring with four clamps attached to it, which will hold the steering wire rope. The first concept, shown in Figure 5.3 A shows this basic principle. However, this tip needs to have a height of 4 mm to have a large enough surface to be attached to the steering wire ropes. Since this is the minimum overlapping space between two surfaces to withstand deformations. The desired height of the tip is as small as possible. Since the smaller the tip, the less surface of the wire ropes will touch the tip and not the ring magnet, and then the wire ropes will be more attracted to the ring magnet. The

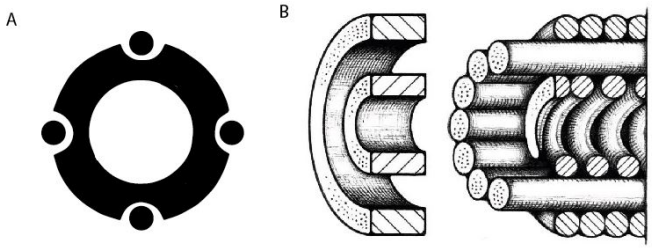

Figure 5.1: (A) Section view of the steerable device of N. van de Berg [23], in which the device is shown and the four steering wire ropes (both in black). (B) Cross section of steerable endoscope of P. Breedveld. On the left, the two rings are shown between which the wire ropes are squeezed. These wire ropes are shown on the right between an inner and outer spring [7].

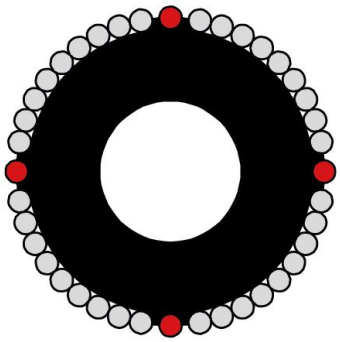

Figure 5.2: The tip (shown in black) which is attached to the four steering wire ropes (shown in red). Between the steering wire ropes the outer wire ropes (grey circles) are positioned which are responsible for locomotion of the flexible shaft.

problem with concept B, shown in Figure 5.3 B is that the steering wire ropes will not be positioned in the same circle around the tip compared to the other outer wire ropes. This is not possible as all these wire ropes need to be positioned in the same circle when they are attracted to the magnet. To decrease the height of the tip, concept C (shown in Figure 5.3 C) was created. In this concept the steering wire ropes are attached to the tip in a groove as well, to minimise the height of the tip but to obtain a glued surface between the tip and the wire ropes of 4 mm.

Another concept to attach the steering wire ropes to the tip is by drilling holes in the tip, in which the wire ropes can be glued. This drilling of a hole can be done in a normal direction to the surface (shown in Figure 5.3 D) or with an angle (shown in Figure 5.3 E) The advantage of concept E compared to D is that the height of the tip can be decreased as the path of the drilling hole is larger than the one of concept D. To obtain the 4 mm length surface between the wire and the tip, the height in this concept can be made smaller. The clamps are still placed at the tip to increase the clamping surface. Subsequently, concept C and E are possible with a smaller height than the other three concepts, which is preferable. Therefore concept C and E are the best options. Using the tip of concept C, it is harder to attach the wire ropes to the tip, because in concept C the wire ropes are attached to the tip only by glue (shown in

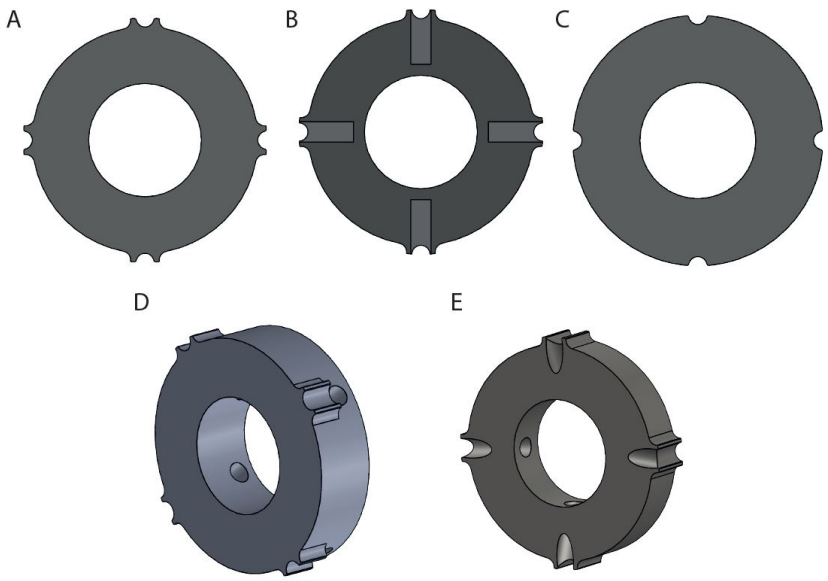

Figure 5.3: Five different concepts of the tip. In each tip, the four steering wire ropes are attached to the tip differently. (A) A ring with four clamps. (B) A ring with four notches. (C) A ring with four grooves. (D) A ring with four clamps and four straight holes. (E) A ring with four clamps and four oblique holes.

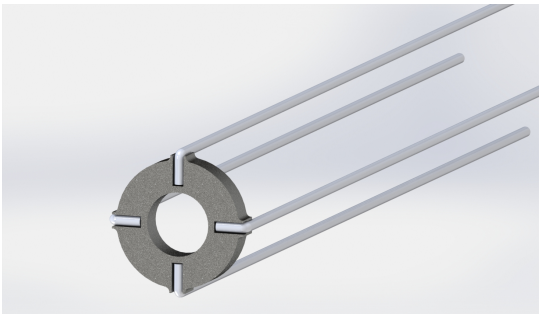

Figure 5.4: Tip design C including steering wire ropes.

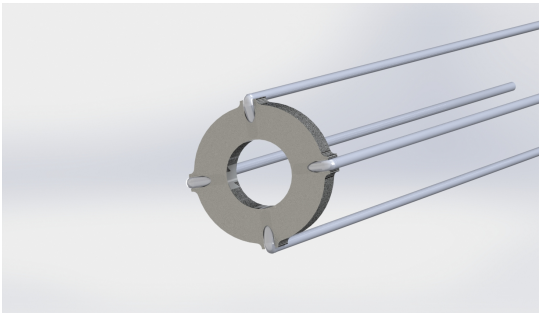

Figure 5.5: Tip design E including steering wire ropes.

Figure 5.4). In concept C the wire ropes can be bend in a way that they can be placed in the holes of the tip and also be glued to the tip, which is shown in Figure 5.5. In concept E, the wire ropes will be also glued to the tip, but by bending them and place them in the holes, it is expected that they already stay attached to the tip without glue. Therefore, concept E is chosen to be the final concept for the tip.

5.2. Final design

The final design, a developed version of concept E, is shown in Figure 5.7. The technical drawing of the tip can be found in Appendix E. When the four steering wire ropes are glued to the tip they can change the direction of the flexible shaft by pulling these wire ropes. In figure 5.6 the tip is shown when added to flexible shaft presented in Chapter 2. The prototype of the tip including the inner wire ropes, outer wire ropes and steering wire ropes is shown in Figure 5.8 and Figure 5.9.

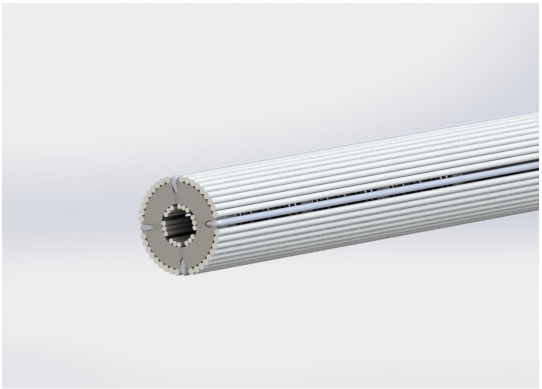

Figure 5.6: Flexible shaft including the steering tip (grey) connected to the steering wire ropes (light grey). The inner wire ropes and outer wire ropes are shown in white.

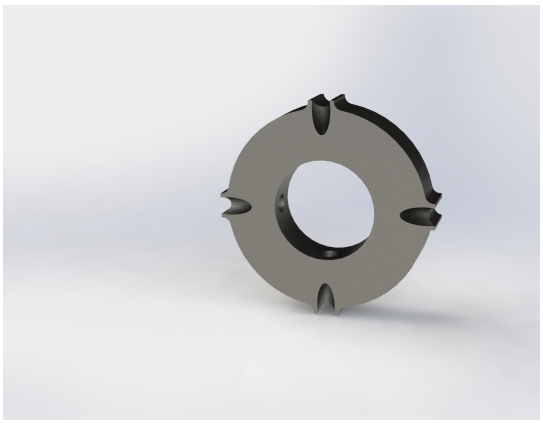

Figure 5.7: Final tip with four holes for the steering wire ropes.

Figure 5.8: An isometric view of the flexible shaft with the tip and the four steering wire ropes included. Behind the tip a ring magnet and compression spring are shown which surround the inner wire ropes.

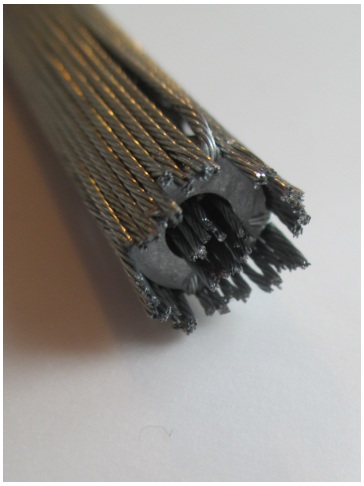

Figure 5.9: An isometric view of the flexible shaft with the tip and the four steering wire ropes included. The inner wire ropes and outer wire ropes are shown as well.

6

Validation of the design

6.1. Experiment: Locomotion

Goal of the experiment

To validate the concept of locomotion through a tube, the following experiment has to be executed. The goal of this experiment is to show that the flexible shaft can locomote through a tube by using the designed actuation system and obtain the locomotion rate of the shaft.

Experimental variables

Independent variable The independent variable is the curve of the tube. The flexible shaft will be tested locomoting through a straight tube (bending radius = infinity) and trough different curved tubes with a bending radius of 130 mm, 105 mm and 80 mm, and an angle of 15°, 30 ° and 45°, respectively.

Dependent variable The dependent variable of the experiment is the locomotion rate of the flexible shaft through the tube, which is the distance the flexible shaft locomotes during one cycle [mm/cycle]. One cycle is equal to one rotation of the cam.

Experimental facility

To move the wire ropes in a way that the shaft will locomote through the tube, the sliders which are connected to these wire ropes will move back and forth by rotating the cam with the attached handle. The design described in Chapter 4 is used to actuate the wire ropes. The actuation system is placed in a holder which is laser cut from 5 mm PMMA. In this way, a person can rotate the cam to move the wire ropes. The flexible shaft is placed above a graph paper from which the length of the transported shaft can be read.

To mimic an organic tube, a transparent tube with a diameter of 12 mm is used [1]. However, this diameter is a few mm wider than the outer diameter of the flexible shaft (11.6 mm). Therefore a heat shrinking tube [2] was glued on the inner surface of the tube to increase the diameter. In this way, the locomotion wire ropes can locomote through the tube by friction.

Experimental protocol

The actuation system will be placed in such a way that the tip is positioned in front of the tube. The length the flexible shaft will move through the tube depends on the bending radius, as shown in Table 6.1, as each curvature has a different length. The number of cycles, which is equal to the number of turns of the cam, will be counted. The four experiments with different bending radii and bending angles will be repeated six times.

Data analysis

The locomotion rate, the distance the flexible shaft will transport through the tube during one cycle, can be calculated by the distance the shaft locomoted divided by the number of cycles needed. See

Table 6.1: The bending radii, bending angles, length of the tube and frequency of locomotion experiment.

Bending radius	Angle	Length	Frequency
infinity mm	0°	103 mm	6
130 mm	15°	103 mm	6
105 mm	30°	69 mm	6
80 mm	45°	86 mm	6

Equation 6.1

$$Locomotion\ rate[\frac{mm}{cycle}] = \frac{locomotion\ distance[mm]}{cycles[-]} \tag{6.1}$$

The average locomotion rate for the different bending radius will be calculated and be presented together with the standard deviation in a graph. This graph is obtained by using Matlab, the file can be found in Appendix B.3. A one way ANOVA test between the four datasets will be performed to test the correlation between the locomotion rate and the bending radius. When the P-value is smaller than 0.05 it indicates that there is at least 95% certainty that there is a difference between the locomotion rates.

6.2. Experiment: Tissue transport and locomotion combined

Goal of this experiment

The goal of this study is to locomote to the target through a tube and transport this tissue out of the body. In this experiment it is shown that the desired steps are possible, which were already described in Chapter 2:

1. Insert of the flexible shaft into the tube
2. Move to the target by the locomotion of the outer wire ropes
3. Transport tissue by the inner wire ropes

In this experiment, it will be validated that all these steps can be executed.

Experimental facility

6.1 mass % gelatin is used to mimic a polyp [13, 21]. This percentage is obtained by combining these references and is shown in Appendix B.2. The actuation part of the prototype is placed in a holder which is laser cut from 5 mm PMMA. The locomotion wire ropes will move through the transparent tube with glued heat shrinking tube on the inner surface. This tube is in a straight configuration.

Experimental protocol

The flexible shaft will locomote through the 40 mm long tube, by rotating the outer cam. When the target location is reached, the gelatin will be placed in the central lumen, such that the is tissue is enclosed by the tissue transporting wire ropes. This gelatin will be transport by rotating the inner cam.

6.3. Experiment: Steerability

Goal of this experiment

In this experiment, the amount of force needed to pull on one steering wire rope to steer the flexible shaft is obtained. The flexible shaft can be steered by pulling on the steering wire ropes. As the required angle of the deflection of the flexible shaft is 90°, the tested bending angles will be 30°, 60° and 90°, with a bending radius of 103 mm, 78 mm and 58 mm respectively.

Experimental variables

Independent variables The angle by which the flexible shaft is deflected and the bending radius of deflection. A1= 30° and 103 mm, A2 = 60° and 78 mm, A3 = 90° and 58 mm.

Dependent variables The dependent variable for this experiment is the force needed to steer in the three different angles [N]. This force is measured with a spring scale.

Experimental facility

The test setup is shown in Figure 6.2. The flexible shaft is placed on graph paper with the indicated angles, shown in Figure 6.1. The spring scale will be pulled and they indicate the needed force of the desired deflection. One hand will hold the flexible shaft at the position of the black rubber band (shown in Figure 6.2), which is 6.7 mm from the tip of the shaft. On the shaft, a split pen is placed which indicates the deflection of the shaft, such that it can be checked whether the desired angle is reached.

Experimental protocol

The spring scale is attached to one of the wire ropes which is attached to the tip. This scale is pulled by hand until the desired deflection is reached. Each of the four steering wire ropes is deflected by each of the three bending radii and is repeated six times. The total number of force measurements is shown in Table 6.2.

Table 6.2: The different steering wire ropes, bending radii, bending angles and frequency of the experiments of the steerability experiment.

Steering wire rope	Bending radius	Angle	Frequency
1	103 mm	30°	6
	78 mm	60 °	6
	58 mm	90°	6
2	103 mm	30°	6
	78 mm	60°	6
	58 mm	90°	6
3	103 mm	30°	6
	78 mm	60°	6
	58 mm	90°	6
4	103 mm	30°	6
	78 mm	60°	6
	58 mm	90°	6

Data analysis

In total, the force needed to deflect the flexible shaft by a certain bending radius has been measured twenty-four times, six times by each wire rope. This results in an average force needed to deflect the flexible shaft by a certain angle. This average force with standard deviation will be shown in a graph, which is executed by Matlab and the script is shown in Appendix B.4.

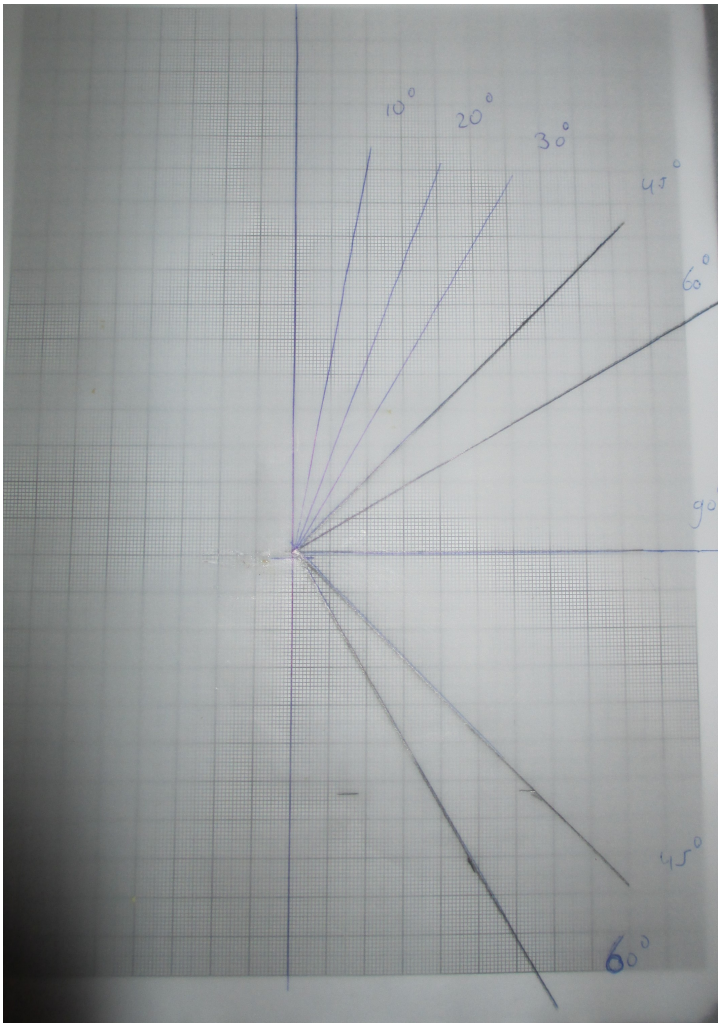

Figure 6.1: Graph paper with the indicated bending angles of the experiment: 30°,60° and 90°.

Figure 6.2: The test setup. The flexible shaft is shown with a black rubber band and the springs scale which is attached to one of the steering wire rope.

7 Results

7.1. Experiment: Locomotion

The raw data of this experiment can be found in Appendix D.1. The graph in Figure 7.1 shows the mean locomotion rate and the standard deviations of the different bending radius of the tube. The mean locomotion rate through a tube with a bending radius of 80 mm and a bending angle of 45° is 5.21 mm/cycle with a standard deviation of 0.21 mm/cycle. If the bending radius is increased to 105 mm and the bending angle is decreased to 30°, the mean locomotion rate is 5.65 mm/cycle with a standard deviation of 0.21 mm/cycle. The mean locomotion rate through a tube with a bending radius of 130 mm and a bending angle of 15° is 4.81 mm/cycle with a standard deviation of 0.43 mm/cycle. When the tube is in a straight configuration (bending radius of infinity mm), the locomotion rate is 6.17 mm/cycle with a standard deviation of 0.27 mm/cycle.

Performing a one way ANOVA test between these four data sets resulted in a P-value of $1.28 * 10^{-6}$. As this P-value is smaller than 0.05, there is a statistically significant difference between the transport rate when locomoting through tubes with a different bending radius. The graph in Figure 7.1 does not show a clear relation between the bending radius and the locomotion rate. The average locomotion rate for a tube with a bending radius of 130 mm shows an unexpected value when looking at the other results and has a higher standard deviation as well.

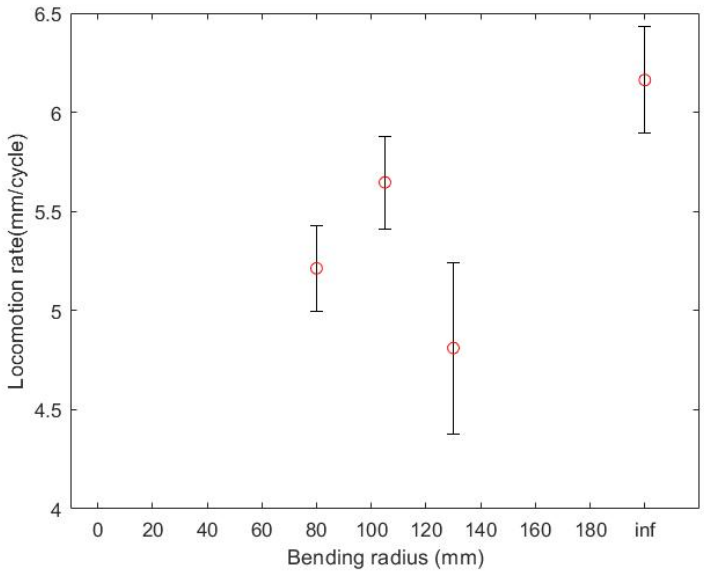

Figure 7.1: Graph showing the locomotion rate for different bending radii: 80 mm, 105 mm, 130 mm infinity.

7.2. Experiment: Tissue transport and locomotion combined

During this experiment the intended use of the flexible shaft are shown:

1. The needle is inserted into the a 12 mm ⌀ tube, which can be seen in Figure 7.2a
2. The needle locomotes through the tube, shown in Figure 7.2b. 7.2c and 7.2d.
3. The target is reached 7.2e
4. The gelatin of 6.1 weight% is inserted 7.2f
5. The gelatin is transported 7.2g, 7.2h and 7.2i.

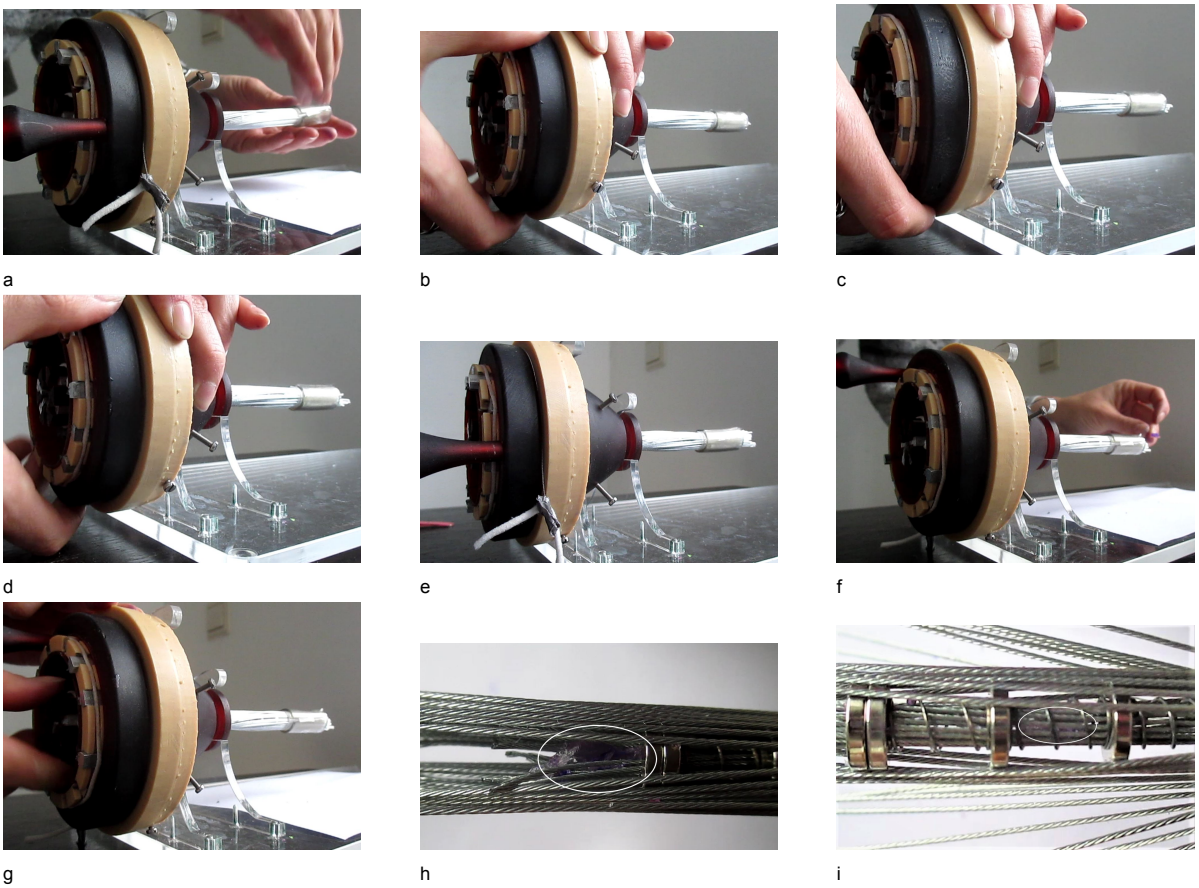

Figure 7.2: Steps of locomotion and tissue transport of the flexible shaft: (a) Insertion into the tube. (b) - (d) Locomotion of the flexible shaft. (e) Reaching the target. (f) Insertion of the Target. (g) Tissue transport. (h) Tissue start location. (i) Tissue final location.

7.3. Experiment: Steerability

The graph in Figure 7.3 shows the mean needed force to deflect the flexible shaft with the desired angle and the standard deviation. The mean force to deflect the flexible shaft by 30° with a bending radius of 103 mm is 10.08 N±0.62N. The mean force to deflect the flexible shaft with 60° with a bending radius of 78 mm is 13.68 N±0.80N. The mean force to deflect the flexible shaft by 90° with a bending radius of 58 mm is 16.34 N±1.29 N. The graph shows a clear relation between the force and the bending radius. All these relative standard deviations are in the same range. Therefore these results were obtained with the same precision. The raw data of the experiment can be found in Appendix D.2.

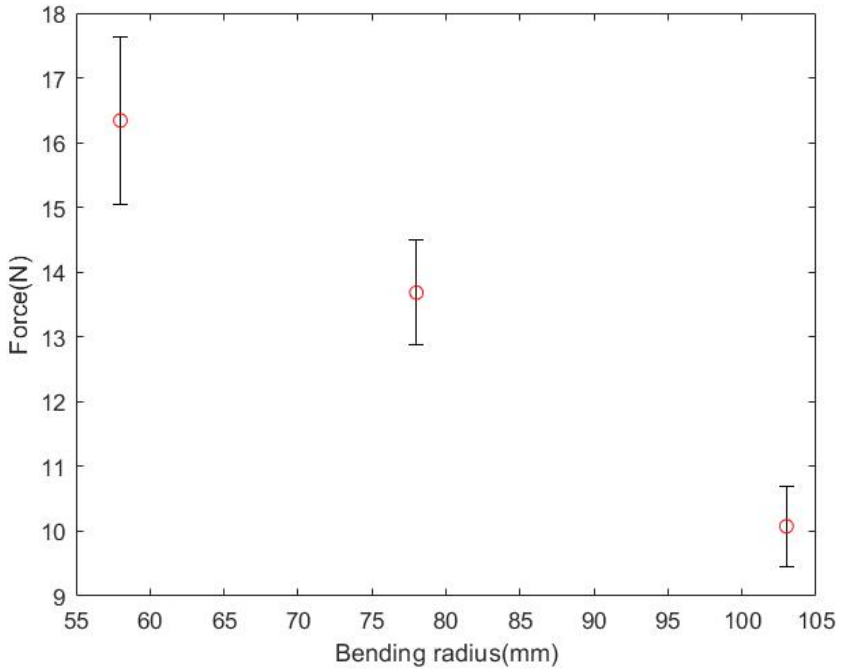

Figure 7.3: Graph showing the needed force to deflect the flexible shaft by a different bending radius: 58 mm, 78 mm and 103 mm.

8

Discussion

8.1. Main findings

In this study, a flexible shaft with a friction-based transport mechanism was created which can locomote through a tube and, after reaching the target area, transport tissue. The mechanism of this design was inspired by the ovipositor of a parasitic wasp, a tubular organ that can deposit and transport the eggs of the female wasps. The wasp-eggs are transported by friction-based transport. Inspired by this friction-based transport mechanism, a flexible shaft was created that can locomote through a tube and, after reaching the target area, transport tissue. The locomotion of the designed flexible shaft is done by rotating the outer cam which is responsible for the back and forth movement of the wire ropes in the outer ring. The total length of this flexible shaft is 203 mm, has an outer diameter of 11.6 mm and an inner diameter of 3.8 mm. The prototype consists of an inner ring of eighteen wire ropes which are responsible for tissue transport. The outer ring consist of forty wire ropes, thirty-six of them are responsible for locomotion and four wire ropes are responsible for the steering of the flexible shaft. The inner ring shapes the lumen through which the tissue is transported due to its attraction to the ring magnets. Between these ring magnets compression spring are positioned, which surround the inner wire ropes. On the outer surface of these magnets and compression spring, the locomotion wire ropes and steering wire ropes are positioned due to the attraction to the ring magnets. These wire ropes form the outer ring of the flexible shaft. The inner ring is actuated by rotating the inner cam and the outer ring is actuated by rotating the outer cam. Together these cams form the actuation of the flexible shaft.

In the locomotion experiment, it was shown that the flexible shaft can locomote through a tube in a straight position and three different curved positions: with a bending radius of 80 mm, 105 mm, and 130 mm and a bending angle of 45°, 30° and 15°, respectively. The flexible shaft has the highest locomotion rate when it locomotes through a straight tube: 6.17 ±0.27 mm/cycle and the lowest locomotion rate when locomotion through a tube with a bending radius of 130 mm: 4.81 ±0.43 mm/cycle. Using a one way ANOVA test it was shown that the difference between these locomotion rates is statistically significant. The observed decreased locomotion with lower bending radii as expected, since the wire ropes will be forced to locomote along a bent shape while these ropes want to locomote in a straight direction, as their initial shape is in a straight configuration.

During the locomotion of the flexible shaft through the bent tubes, the springs were compressed. This causes the flexible shaft to not locomote further after a few rotations. This happened more often when the shaft locomotes through a bent tube instead of a straight tube. The compression of the springs is thought to cause a decrease in locomotion rate when locomoting through the bent tubes. However, the results of the tube with a bending radius of 130 mm were an exception for this, since the locomotion rate is lower compared to the tube with a bending radius of 105 mm. This was caused by the glued heat shrinking tube to the tube, the heat shrinking tube surrounded the shaft in such a way that the flexible shaft locomotes less easily through it than through the other curved tubes. It surrounded the shaft too tight or too loose. When it was too tight, resistance was created between the wire ropes and the heat shrinking tube, which decreased the locomotion rate. When the heat shrinking tube was too loose, less friction was created between the wire ropers and the heat shrinking tube, which would decrease the locomotion rate as well. The results of the locomotion rate with a bending radius of

105 mm have a higher standard deviation than the other bending radius as well. The results of the locomotion experiment show that the friction between the outer wire ropes and the surface of the bent tube differs a lot between each rotation of the outer cam.

In the locomotion and tissue transport combined experiment it was shown that the flexible shaft can be inserted into a tube, locomote through this tube and subsequently transport tissue. After the target is reached, the tissue phantom: gelatin 6.1 weight% was inserted into the lumen. To transport this gelatin, the inner cam needed to rotate to move the tissue transport wire ropes back and forth. In this way, the tissue could be transported out of the body. All these steps are possible with the current prototype. However, it was difficult to insert the gelatin into the lumen due to the deflected wire ropes.

In the steerability experiment, it was shown that the flexible shaft needs a pulling force of 10.08±0.62 N on one of the steering wire ropes to bend it by a bending radius of 103 mm and a bending angle of 30°. A pulling force of 13.68 ±0.8 N was needed to create a bending radius of 78 mm and a bending angle of 60°. And 16.34 ±1.29 N was needed to create a bending radius of 58 mm and a bending angle of 90°. The force required to obtain the desired bending radius has high accuracy.

8.2. Limitations of the experiments

Sample size During the locomotion experiment, the flexible shaft was locomoted six times through each different bending radius. During the steerability experiment, each steering wire rope was deflected in each bending radius six times as well. Since both experiments were performed a limited number of times, more accurate data could be obtained by increasing the number of measurements per experiment.

Measurement setup errors During the experiments, a lot of things were measured using a ruler: the bent tubes, the locomoted path of the flexible shaft through the tube and the bending radii. The ruler had a precision of 0.5 mm. Also, the curved length of the tube was measured by using a string which was placed next to a ruler to measure this length. As this included two steps, it is less accurate than measuring the bent path with a string that would have lengths on it.

Material of prototype The material that was used to manufacture the prototype was material that is off the shelf. The prototype could be redesigned using materials with dimensions that would be more appropriate. As the diameter of the current compression springs was too large to shape around the inner wire ropes, the experiment can be improved by using compression springs from which the diameter and thickness can be chosen such that they will fit between the two rings of wire ropes perfectly. Additionally, these compression springs could be manufactured in a way that their spring rate differs more to create a more flexible tip and a stiffer section of the shaft close to the actuation system. If ring magnets would be manufactured with a smaller difference between the inner and outer diameter, it would also be possible to decrease the outer diameter of the flexible shaft.

8.3. Limitations of the study

Tissue transport The prototype validated that 6.1 weight% gelatin could be transported through the lumen. However, the wire ropes were partly deformed and therefore hard to put the gelatin into the lumen. As the outer ring wire ropes have the same length as the inner ring wire ropes, it was hard to reach the lumen. Also, parts of the gelatin moved through the small gaps between the wire ropes. The tissue was only transported in a straight configuration, but it has previously been validated that transport with a bending radius of 59 mm is possible [10]. Therefore, it is expected that the prototype of this study can do that as well.

Prototype fitting As two different 3D printers were used, the printed parts were printed with different precision. This resulted in a suboptimal fit of some parts of the prototype, while designed to have a perfect fit. Although the 3D printed designs were changed to improve the fit of the components, still some parts had to be sanded to fit each other and screwed to each other. Another problem was that there was not enough space left for the outer wire ropes to move along the inner cone, but after sanding and pushing the parts together it was possible to assemble the prototype.

8.4. Recommendations for future research

Adding an cutting component The developed design shows potential to locomote through a tubular organ and transport tissue. However, this tissue needs to be cut from the surface of the tubular organ before it can be transported. Therefore, an extra design could be made that can be inserted through the lumen which can be folded out at the tip to cut the tissue, shown in Figure 8.1. This cutting component can be an already existing design, such as a wire loop, shown in Figure 8.1. This wire loop slips over a polyp and during the closure of it, the polyp is cut from the colon wall. Or research needs to be carried out to develop an optimal method to cut tissue when folded out at the tip of the flexible shaft. In this way, the design could execute every step in the process of transporting tissue out of the body to examine it.

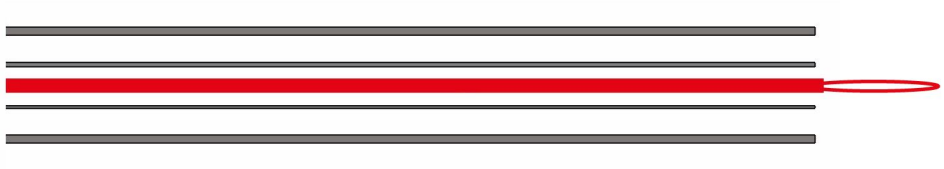

Figure 8.1: A section view of the two rings of wire ropes, each of them is displayed by two grey lines. Through the inner ring (the lumen), an instrument (shown in red) could be inserted which can be folded out (red ellipse) when reaching the target to cut it.

Adjustable outer diameter Since the outer diameter of the design has to touch the surface of a tubular organ to be able to locomote through it, it is desirable to have an adjustable outer diameter. It would be possible to adjust the outer diameter to fit precisely through the tubular organ. This could perhaps be done by adding an extra cover to the outer wire ropes, to increase the outer diameter. In this way, the outer diameter could be adjusted to any outer diameter larger than 11.6 mm, which is the outer diameter at the moment.

Springs and magnets During the locomotion of the flexible shaft, the springs were compressed. This can be explained by the wire ropes moving back and forth not only locomoting the instrument, but also transporting the ring and springs along the shaft. Therefore it was not possible to locomote the flexible shaft through the entire length of the tube. As the moment the springs were maximally compressed, the rotating cam could not rotate any more. The cam could not rotate any more as when the springs were maximally compressed the spring and ring magnets could not be transported along the shaft. This caused the cam to be 'stuck'. During the tissue transport and locomotion experiment, an extra magnet was added to the tip of the flexible shaft, as the tissue transport wire ropes were deformed and also a bit unravelling. This solved this problem a bit already, as the wire ropes needed more force to pull the two magnets than one magnet and therefore the springs and magnet transported less along the shaft. Therefore, it is recommended to investigate further the combination of the compression springs and the ring magnets. One solution could also be to replace the compression spring with an element that can bend but can not be compressed, such as a flexible tube.

Actuation The actuation was designed that by rotating a sling, which is attached to the cam, the tissue transport wire ropes and locomotion wire ropes could be actuated. However, those could not withstand the force needed to rotate the cam. Subsequently, the cams had to rotate by rotating the cam instead of the sling. This is less ergonomic than using a sling to rotate. Another disadvantage of rotating the inner cam without a sling is the limited space between the cam and the inner cone not a lot of space is present, shown in Figure 8.2. In this limited space the fingers of the user are placed around the cam to rotate it. Therefore the actuation of this flexible shaft needs to be redesigned to rotate the inner and outer cam more ergonomically.

Combining the locomotion and steerability In this study, steering wire ropes and a tip of the flexible shaft are presented to add steerability to the flexible shaft. The locomotion of the flexible shaft has been validated and the tip shows potential for steerability. Therefore, in a follow-up study, it is interesting to

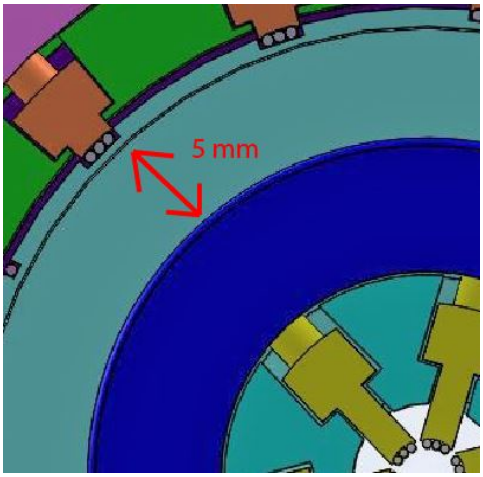

Figure 8.2: The limited space shown between the inner cam (dark blue) and the inner cone (light blue), which is 5 mm. In this space, your fingers need to surround the inner cam to rotate it.

combine these two characteristics. The outer ring will include the steering wire ropes and the locomotion wire ropes. A handle to pull on the steering wire ropes that could be added to the current actuation of the inner and outer ring needs to be designed.

Different method to steer the flexible shaft In Chapter 5 the design is illustrated which can be added to the flexible shaft to make it steerable. It was chosen to add a tip and steering wire ropes to the design. This design was produced by a literature study, which could be found in Appendix C, which compared three existing steerable devices. However, from these designs another method to add steerability to the flexible shaft could be chosen. The outer wire ropes could be programmed in such a way that the flexible shaft would steer to the desired direction by creating a bevel tip [22]. Another method is to add a flexible component into the lumen with a steerable tip, which will cause the flexible shaft to steer [23]. When the target is reached, this component could be removed from the lumen, which makes the lumen available for tissue transport.

Steps toward clinical application This flexible shaft shows potential to locomote through a tubular organ and transport tissue. However, when this instrument would be redesigned to use inside an organism, adjustments need to be made to meet medical requirements. The wire ropes are now made of steel, probably, it will feel more convenient if they are covered by a kind of plastic when it locomotes through a tubular organ. Since the wire ropes will locomote along a surface of a tubular organ, and this could feel less painful with an extra plastic cover around the steel wire ropes. Also, the length of the flexible shaft needs to be increased to reach targets that are further inside the body. Important as well is to redesign the flexible shaft in such a way that it is easier to clean and make sterile when it will be used inside a human body. Therefore it needs to be easier to disassemble and assembly again, which is at the moment hard. It is also a possibility to make the instrument with disposable materials, then it is not necessary to clean it, but for every usage, a new instrument can be used.

9

Conclusion

This study shows the design of a flexible steerable friction-based transport mechanism that can locomote through a tube and transport tissue. In this study, a prototype is manufactured and validated. The prototype consists of an inner ring of wire ropes which is responsible for tissue transport while the outer ring of wire ropes is responsible for locomotion. The flexible shaft is able to locomote through a tube in a straight configuration and three different curved configurations: One with a bending radius of 80 mm, 105 mm and 130 mm which had a bending angle of 45°, 30° and 15°, respectively. When the locomotion is finished, tissue could be transported through the lumen. Therefore it can be concluded that this prototype can locomote through a tube and transport tissue using friction-based transport, which was the goal of this study. This instrument would also be possible to steer up to 90° with a bending radius of 58 mm by adding the tip with steering wire ropes. When pulling on one of the four wire ropes this bending radius is achieved. However, how these wire ropes are actuated needs still to be designed. Furthermore, the prototype needs to be redesigned to meet the medical requirements and to be able to locomote further through a curved tubular organ. This design shows potential for a flexible shaft that is able to transport tissue and locomotes through a tubular organ.

Acknowledgement

I would like to thank all the people who helped me with this graduation project. First of all, I would like to thank my parents, when I was stressed, they always calmed me down. During my time as a student, they always were very supportive and gave useful advice. My complete graduation project took place during the COVID-19 pandemic. This made it extra challenging. Luckily, I always had people to study with during the lockdowns due to COVID-19. Therefore, I would like to thank my study buddies, without them studying would be more challenging and definitely less fun. During the first lockdown, it motivated me a lot that I could study with Sterre and Tjitske every day. Unfortunately, they were already graduated during the second lockdown, so I found new study buddies in Maaike, Eva, Lucie and Jesse. I would like to thanks my friend Aline as well, she gave useful feedback to my thesis, which increased the quality of it. My prototype would not exist without David Jager, the precision mechanics at DEMO. He gave me a lot of recommendations to improve the quality of my prototype. He took the time to explain everything to me and spend a lot of time printing components of my design. During the project, I had two meetings with Prof. Dr. Ir. Paul Breedveld. He gave me useful insights from a different perspective on how to look at the difficulties of my project. I started my graduation project with the same supervisor of my literature report: Dr. Ir. Aimeé Sakes. I would like to thanks Aimée for her great guidance and all her feedback. She helped me a lot with being critical of everything I came up with. When I got stuck with a problem, she asked questions that helped me further and I could continue with the design process. Although we met in person a few times, we had a lot of online meetings during which I could ask and discuss extensively. My second supervisor, Esther de Kater, supervised me together with Aimée. When Aimée went on maternity leave, she continued the guidance alone really well. Every week we had a meeting in which I could discuss everything which was on my mind regarding the project and together we always came up with new ideas or how to solve a problem. She helped me a lot with this report, as she gave useful feedback to it many times. Due to all her feedback, I was able to deliver a clear report, with a good structure. I am really glad that I chose this project together with the supervision of Aimée and Esther, as their guidance during this project was great!

A

Hexasected motion sequence of the Endo-Tubular Friction Carrier

As can be seen in Figure 1.4 the blades all have a letter, starting from A to F in a clockwise direction. This will guide the explanation of the motion of the blade. In Figure A.1 six different steps are shown of the motion sequence. In step 1 the black blade (A) is at the minimum stroke location. The stroke length is the difference between the maximum and minimum stroke location of the blade. While the single black blade is at its minimum stroke location, the other blades are moving backwards in a stepped manner, this means that all of them move backwards while not having the same stroke length, shown in Figure A.1 2. In Figure A.1 2 the single black blade is moved to the maximum stroke length, while the others still move backwards in a stepped manner. Consequently, the five blades move back slower than the one blade moves forward. This backward movement repeats itself, each time another blade is pushed forward while the other five move backwards. As the five blades create more friction between the tissue and the blades than the single blade, the tissue will move in the direction of the five blades.

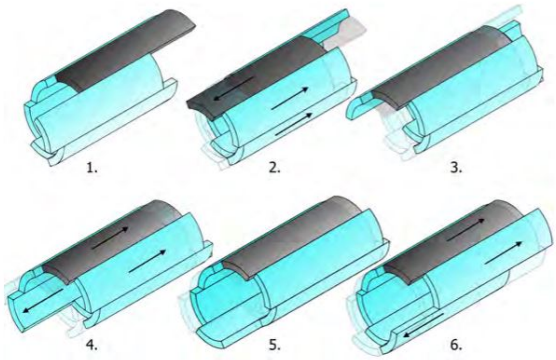

Figure A.1: The different steps of the hexasected reciprocating motion sequence. Five of the blades are blue and one is black. In these six images, it can be seen that each time one single blade (in this case the black one) is at the maximum stroke location, the other ones (the blue ones) is moving gradually back. This sequence is repeated all the time: continuously another blade is pushed forward while the other five move backward[24]

.

B

Matlab files

B.1. Calculation of the amount of outer wire ropes

Calculation of outer and steering wire ropes

```
Dw= 0.8; %mm wire diameter
Dro=10; % mm outer diameter ring magnet
Dri=5 ;%mm inner circle of ring magnet
Dow=Dw+Dro; %mm The diameter of the circle on which the wires will lay
Cwr=pi*Dow ;%mm circumference of the circle on which the wires lay
c=1.28; % clamp dimension
Cwrc=Cwr-4*c;  %circumstance without the four clamps
Nc=Cwrc/Dw %number of cables
```

```
Cwrc4=Cwrc/4; % space in each segment
% 9 cables in each segment
sp=Cwrc4-(9*0.8) ;  %space left in each segment
sp1=sp/10; %space between cables
spc2=sp1+0.8   %solidworks distance between the centres of the cables
spc3=c/2+sp1+0.4 % distance from cable in clamp to cable next to it
```

Calculation of number of inner cables

```
Diw=Dri-Dw;    %mm The diameter of the circle on which the wires will lay
Cwri=pi*Diw; %mm circumference of the circle on which the wires lay
Ni=Cwri/Dw % number of wires
```

B.2. Determination of gelatin weight percentage of the phantom

The gelatin phantom has to mimic a colon polyp. In order to what weight% of gelatin is needed to mimic the polyp, two different references were used. In the supplementary information of the research of M. Scali [21] the Elastic Modulus [kPa] was determined of different weight% of gelatin. These results were fitted using Matlab, shown in Figure B.1. From the other reference, the Elastic Modulus of a polyp was obtained: 7.51 [kPa] [13]. Combining the information of both references resulted that a polyp can be mimicked by preparation of gelatin with a weight of 6.1 weight%.

```
clear all
clc
close all
x= [5 8 10 15]'; %percentage of gelatin
y = [5.3 12 17 31]'; %kPa youngs modulus
format long
b1=x\y;     % calculating the slope
yCalc1 = b1*x;  %fitting the percentage of gelatin
scatter(x,y)   % and the youngs modulus
hold on
% plot(x,yCalc1)
xlabel('Weightpercentage gelatin (%)')
ylabel('Young,s modulus (kPa)')
grid on
X = [ones(length(x),1) x];
b = X\y;
yCalc2 = X*b;
plot(x,yCalc2,'--')
legend('Data','Fitted line')
```

```
percentagepolyp=(7.51-b(1))/b(2)  %calculating the gelatin percentage of polyp
```

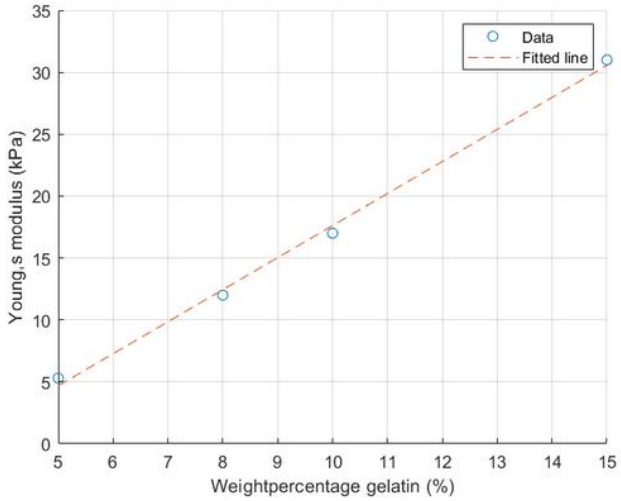

Figure B.1: The plotted data of the results of M.Scali [21]. The blue dots represent the data from her research and the orange dotte line the fitted line.

B.3. Matlab code of experiment: Locomotion

```
locomotion=importdata('Experiment2.mat'); %reading out results
loc=table2array(locomotion);
n=zeros(4,1);
m=zeros(4,1);
for i=0:3
    n(i+1)=mean(loc(1+6*i:6+6*i));  %calculating mean of results
end                                 % of each different bending radius
for j=0:3
    m(j+1)=std(loc(1+6*j:6+6*j)); %calculating standard deviation
end                               %of each different bending radius
x = [200 130 105 80];   % the different bending radius
errorbar(x, n, m, 'ko');
hold all
plot(x,n,'ro');
xlim([-10 220])
xticks([0 20 40 60 80 100 120 140 160 180 200])
xticklabels({'0', '20', '40', '60', '80', '100','120' ,'140','160', '180', 'inf'})
xlabel('Bending radius (mm)')
ylabel('Locomotion rate(mm/cycle)')
```

B.4. Matlab code of experiment:Steerability

```
steeringcables=importdata('Resultatenexperiment.mat');
steerc=table2array(steeringcables); %reading out results of experiment
n=zeros(3,1);
for j=1:4;
for i=0:2;
    n(i+1)=mean(steerc(1+6*i:6+6*i,j)); %calculating mean
end
end
steerc30=steerc(1:6,1:4);   %extracting the results for 30 degrees
steerc30=steerc30(:);
std30=std(steerc30);        %calculating the standard deviation for 30 degrees
steerc60=steerc(7:12,1:4); %extracting the results for 60 degrees
steerc60=steerc60(:);
std60=std(steerc60);        %calculating the standard deviation for 60 degrees
steerc90=steerc(13:18,1:4);   %extracting the results for 90 degrees
steerc90=steerc90(:);
std90=std(steerc90);        %calculating the standard deviation for 90 degrees
x=[103 78 58];                  %the corresponding bending radius for the bending angles
e=[std30 std60 std90];
errorbar(x,n',e,'ko')
hold all
plot(x,n','ro');
xlabel('Bending radius(mm)')
ylabel('Force(N)')
```

C

Literature review steerable devices

C.1. Categorization of steerable devices

In literature, different methods can be found how a device can be steered. These methods can be categorized into the way their path is adjusted, internally and externally. When a device is externally steered their path is is deflected by a source from outside the body, such as a magnet. When a device hits a hard obstacle, such as a bone, and deflect its path by this structure, it is not called external steered. Since the direction is not adjusted by the user but unintentionally by the surrounding of the needle tip. Inside the body, the device can be steered in two different ways: pre-defined and user-defined. Pre-defined means that the tip of the device is adjusted before entering the body in such a way that way they are steered in the right direction. When a device is user-defined the user can adjust the direction of the needle during the insertion and locomotion of the needle. In the two categories, pre-defined and user-defined different examples are illustrated. The flow diagram of the categorization is shown in Figure C.1. As the demand for this instrument is that is can be actively steered, therefore

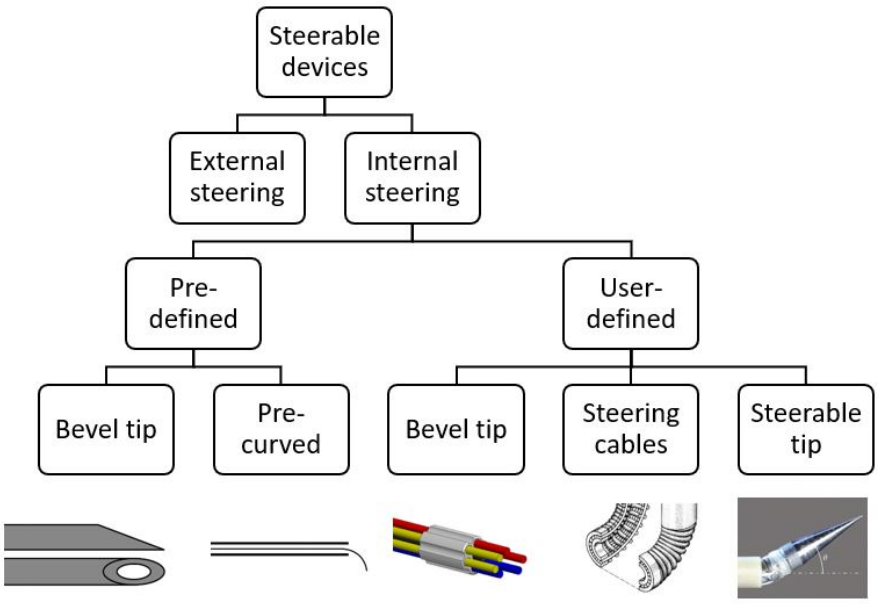

Figure C.1: Flow diagram of the categorization of steerable devices [8, 22, 23].

the three user-defined devices will be discussed below. They are compared to each other and one design will be chosen. This design will be used as a reference from which the design of this research will be developed.

C.2. User-defined steerable devices

C.2.1. The programmable discrete bevel tip

In the steerable needle design of M. Scali *et al.* [22] a design is proposed which is inspired by the ovipositor of the wasp. The needle consists of seven nickel titanium wires which are held together by two types of rings: a flower-shaped interlocking ring and five standard rings. The flower-shaped interlocking ring is placed close to the tip of the seven wires, this ring aligns the wires and keeps them together. This flower-shaped interlocking ring has seven holes. One hole is situated in the middle and the other six are arranged in a circle around that hole. Through the holes, the wires are placed. The middle wire is glued to the flower-shaped ring and the others can slide through the holes. Each of the six movable wires is connected to a slider that can move backwards and forward by a bipolar stepper motor in conjunction with a lead screw. The wires and flower-shaped ring configuration are shown in Figure C.2a and b. The needle can steer by adjusting the shape of the needle tip. All these wires have

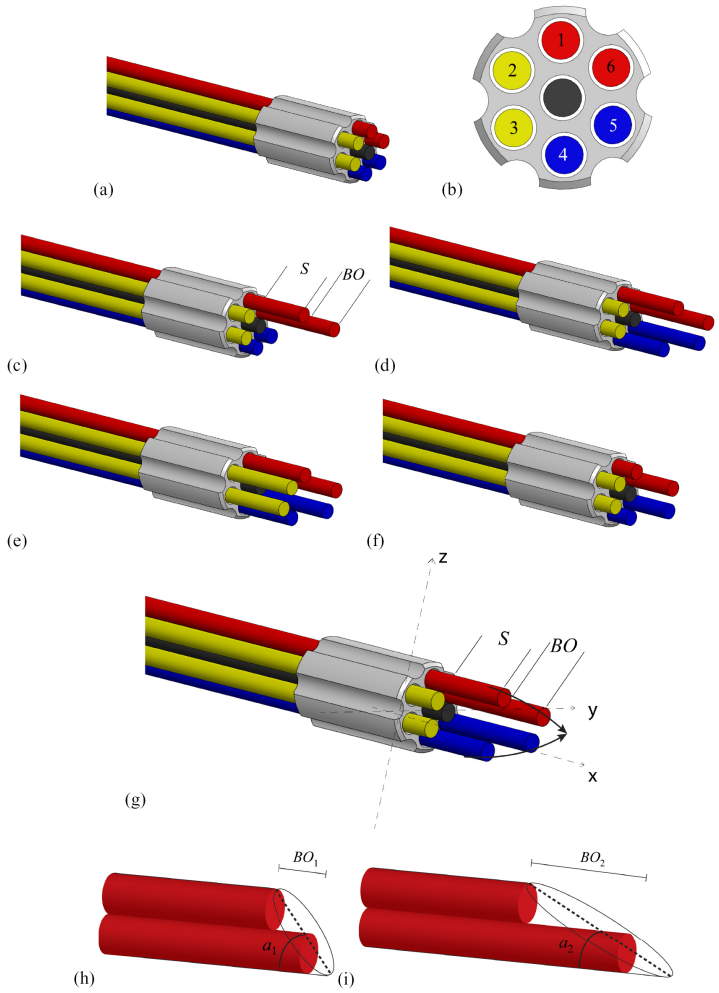

Figure C.2: (a) Initial position of the wires. (b) Cross-section of the needle. (c) - (f) Steps of steering the needle. Steering to the left is done by first creating a discrete bevel between wires 1-6 (red). This is done by setting a bevel offset (BO) between them. (c) These two wires are then advanced by stroke, S. (d) A second discrete bevel is set between wire 5 and 4 (blue) with setting the same BO between them and moves with S. (e) Wires 3 and 2 are then pushed with the same stroke, S. (f) The final step is the pulling of all six wires to let the ring advance. (g) Schematic representation of the needle tip showing the steering mechanism. (h) Discrete bevel tip with angle $\alpha 1$ and $BO1$. (i) Discrete bevel-tip with angle $\alpha 2$ and $BO2$. $BO1 > BO2$. A large BO corresponds to a small angle, this means that $\alpha 2 < \alpha 1$.

a flat tip. However, by adjusting their configuration, a bevel tip can be created from the six wires. A bevel tip can be created by generating an asymmetry at the needle tip. This is done by inducing an offset (called bevel offset, BO) between a pair of adjacent needle wires. This configuration is called a 'discrete bevel-tip' [22]. The steering is performed by executing different actuation steps that are shown

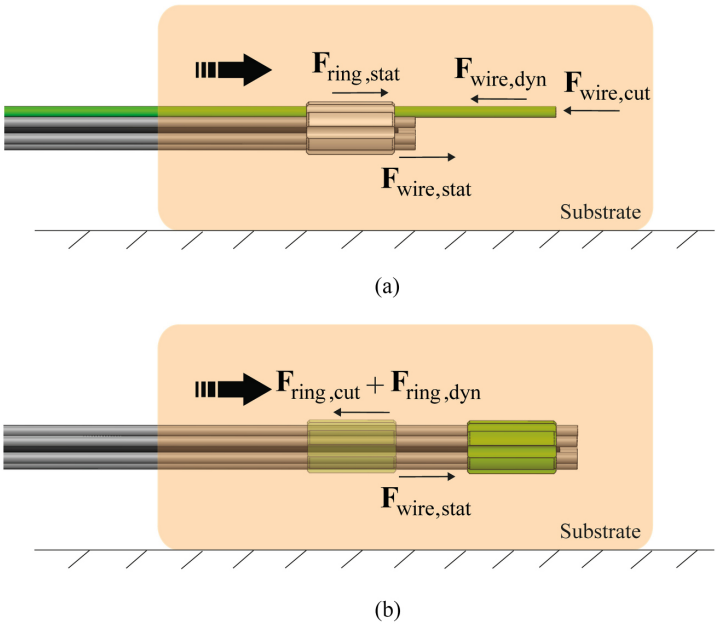

Figure C.3: Schematic representation of the forward motion of the discrete bevel tip. (a) The wires are pushed forward one by one, showing the first wire being pushed. (b) After all these six wires moved forward, they are pulled back together simultaneousy, which results in forward motion of the ring and central wire. The thick black arrow indicates the forward motion of the wires and the ring [22].

in Figure C.2. The first step of executing the needle is to set a bevel offset (BO) between two adjacent wires. This configuration of the bevel tip is advanced to a stroke, S (predefined distance), shown in Figure C.2 c. The needle is deflected and creates a curved path in the substrate [22]. The next step is to set the BO between two adjacent wires which are situated next to the first two wires. These wires then are also advanced for S (shown in Figure C.2 d). This supports the curved path set by the first pair of wires. After this is done, the two remaining wires are advanced over S, following the same curved path as the two other pairs (Figure C.2 e). The last step is to pull these six wires backwards at the same time (Figure C.2 f). In this way, the seventh (central) wire and the interlocking flower ring move forward along the curved path [22]. This forward motion is shown in Figure C.3. In Figure C.3 a the forces are shown which act on the needle when one wire is pushed forward. These forces will not be explained in detail as the focus is on the steering of this design and not the moving forward of it. In Figure C.3 b it is shown when all the six wires are pulled back at the same time, the ring and central wire will move forward (illustrated with the black arrow). The direction of the steering can be set by choosing which pair of wires will form the bevel tip. Steering to the left is done, for example, by setting a BO between wires 1 and 6, the second bevel tip consists of wire 4 and 5. This method can also be used to steer any other desired direction. The first bevel is created by setting a BO between wires 1 and 2 and the second bevel tip is created wire 3 and 4 [22]. With this discrete bevel tip, it is possible to create different bevel angles. For example, moving the wire forward over an offset $BO1$ a angle $\alpha 1$ is generated (Figure C.2 h), while by moving a wire over an offset $BO2 > BO1$, a bevel angle $\alpha 2 < \alpha 1$ is created (Figure C.2 i). This means that creating a larger offset will lead to a smaller steering angle.

Limitations of the design

- Precurvature of the wires, therefore the needle had a preference steering to the right although the needle was steered to the left.
- Bifurcation of the wires when the needle is advanced through the tissue. They slide through the flower shaped interlocking ring, but how further they are pushed from this ring they will divide from each other.
- In this research they assumed that needle deflection only occurs in the steering plane, which is preferable. However, during the experiment with the needle, it was observed that the needle

tended to deflect upward. This could also be caused by pre-curvature of the wires or vertical misalignment in the phantom [22].

C.2.2. Parallelogram-mechanism

In the research paper of P. Breedveld *et al.* [8] a steerable endoscope for laparoscopic surgery is presented. This endoscope is inspired by the tentacles of a squid. This prototype consists of 22 cables which are kept circular by an inner and outer spring. In this way, radial displacements are eliminated. Between the inner and outer spring, a ring-shaped slot is created through which the cables can be guided. This slot is completely filled with cables (cross-section of it shown in Figure C.4, in this way the cables are fixed in tangential position as well[8].

Steering of the tip is done by a spatial parallelogram-mechanism (shown in Figure C.5). At the tip, the cables are fixed between two rings. The cables can be shafted through the shaft and at the handgrip they are fixed between two other rings. These rings form a carriage that can slide in the handgrip. Inside the cable ring, a spring is positioned (along the entire length of the cables). The cable ring, indicated with a in Figure C.5 is surrounded by three springs: a tip spring (c in Figure C.5), a handgrip spring (d in Figure C.5) and a compensation spring (e in Figure C.5) in the handgrip [8]. These four springs (the inner spring and the three outer springs) keep the cables in position and prevent buckling as well. The tip spring is less strong than the compensation spring. Bending the handgrip can determine the releasing of the cables, as when it is bent, part II (shown in Figure C.5) of the cable (which is positioned at the outside of the curvature) becomes longer. But part I (shown in Figure C.5) of that cable cannot become shorter, as the tip spring is compressed. Therefore, Part III (shown in Figure C.5) becomes shorter and the carriage moves downward. This leads to releasing of the other cables, these will slide through the handgrip and shaft. As a result, the tip spring will bend with a very small radius until it reaches the same bending angle of the handgrip [8].

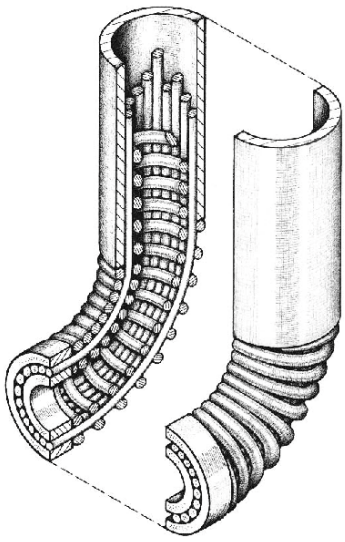

Figure C.4: A cross section of the tip of the endoscope [8].

Limitations of the design

- When this needle is bend, the springs will we compressed. This leads to a decrease in the bending radius and the cable-ring mechanism will be constructed and the manoeuvrability of the tip will decrease [8].
- The steering cables must be kept under tension to use them.
- A drawback of this system compares to spine mechanisms is that the torsion stiffness is lower [8].

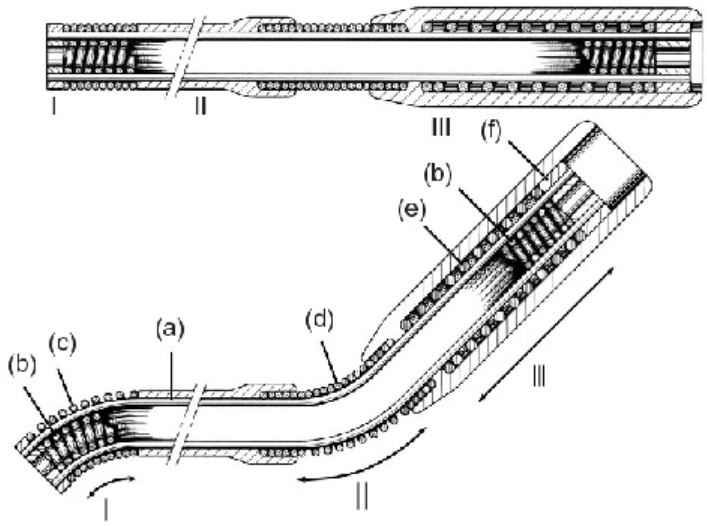

Figure C.5: A cross-section of the parallelogram-mechanism of the endoscope in the straight (top) and bent position (bottom). The endoscope is divided into three parts: (I) the tip, (II) the shaft) and (III) handgrip. The different components of the system are indicated with: (a) cable ring, (b) inner spring, (c) tip spring, (d) handgrip spring, (e) compensation spring and (f) carriage [8].

C.2.3. Steerable tip design

Steering the needle can also be done by adding a deflecting tip to a cannula, which is a tube that can be inserted into the body. In this way, only the tip can deflect instead of the complete needle. This is done in the design of Van De Berg *et* al. [23]. The needle is composed of a flexible cannula which is connected to a conical tip by a ball joint. Inside the cannula a stylet is present, this stylet can be withdrawn after placing the needle, which leaves an open lumen inside the cannula. The ball joint is tendon driven; in this design, it means that the ball joint is attached to steering cables which are actuated to deflect the tip. In this way, the needle can follow the curved path initiated by the rotated tip. In the design of Van de Berg *et al.* the ball joint is actuated by four cables. These cables are actuated by servo motors which work in complementary pairs. The conical tip can rotate with two rotational DoF which is caused by alteration of the servo positions. In this way, the needle can be steered in any direction. These motors are fixed on a linear stage that inserts the needle and this provides a 3 DoF system [23].

The needle (170 mm) consists of stainless steel stylet (⌀ 1 mm) which has three grooves for optical fibres. This stylet is inside the cannula (⌀ 1.8 mm) which has four grooves for the steering. A layer of PET plastic covers the grooves and the cables in place. The outer needle radius is approximately 1 mm [23]. The four steering cables are fixed at the tip and run over the ball joint, along the cannula and exit the needle hub. This configuration is shown in Figure C.6. All these cables are connected to a servo motor by a rack. These racks allow tip rotations (steering magnitude ϕ) of approximately 20° [23]. In this design, optical fibres are implanted in the needle stylet to reduce the target error. This stylet is removed after placement and the cannula can be used as a transport channel.

Limitations

- The cannula was not perfectly straight (radius of curvature in the order of 10 m). However, it was noticed during testing the prototype that this can be compensated. Since the tension levels in the steering cables will affect the friction of the ball joint. When the normal force is above a certain threshold, stick-slip friction will prevent joint rotations and allows the cannula to bend during actuation. In this way, it will compensate for the pre-curvature.

- The steering response is very sensitive to inaccuracies, as the position tolerance is high of the cable fixations. These cable fixations determine the transmission between the linear displacement and the tip rotation [23].

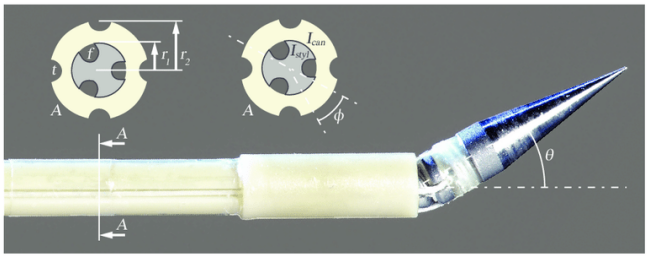

Figure C.6: The steerable needle with the stylet of radius r_1 with grooves for optical fibres (f). The cannula with radius r_2 and grooves for the steering cables (t). The tip angle is indicated with θ which can be altered in any direction ϕ [23].

C.3. Comparison of the steerable devices

Three different used-defined designs were described in the previous sections. One with the programmable discrete bevel tip which can be adjusted to steering any direction. The second design steers by pulling and releasing stirring cables. These are kept in position by i.a. springs. The third design steers with the help of steering cables which manipulate the direction of the tip. One of the three designs will be chosen to develop further. The comparison between the designs is displayed in Table C.1

Table C.1: Comparison of different characteristics between the three designs.

	Bevel tip	**Parallelogram-mechanism**	**Steerable tip**
Maximum steering angle	4.4 °	60 °	20 °
Bending radius	543.47 mm	$\pm$ 58 mm^{-1}	10 m
Diameter	1.2 mm	5 mm	2 mm
Compliant needle	Yes	Yes	No
Accuracy	Unknown	Unknown	6.2 ± 1.4 mm
Precision	Unknown	Unknown	2.6 ± 1.1 mm
Sensing gear	No	No	Yes
Adjustment possible during insertion	Yes	Yes	Yes
Control	Stepper motors	Handgrip	Servo motor
Open lumen	No	Yes	Yes
Precurvature	Yes	No	Yes
Number of cables	7	22	4
Cables in tip	Yes	Yes	No
Shape of tip	Bevel	Flat	Conical
Integration open lumen possible	Yes	Yes	Yes
Bifurcation	Yes	No	No

- The steering angle is significantly smaller at the bevel tip design compared to the other two designs. Only the parallelogram-mechanism meets the demand for the steering angle.
- The diameter of the endoscope of parallelogram-mechanism is notable larger than of the other two. However, this design is also possible with a diameter of ⌀ 0.9 mm [6], in a follow-up design of the parallelogram-mechanism: the master-slave design[12]. However, this diameter is smaller than the demanded diameter.
- The accuracy and precision is not known from two of the three designs, therefore they can't be compared to each other.
- The bevel tip design and the parallelogram-mechanism design consists of different components which constitute the needle. This needle is compliant. The steerable tip design, however, consists of different components which constitute two different parts of the needle, the cannula and the

tip. These parts aren't compliant. Therefore the steerable tip design does not meet the demand of being compliant

- The parallelogram-mechanism is the easiest to control, as this is done with a handgrip and meets the demand of being easy to control. The other two designs are controlled not by the user, but by a servo or stepper motor.
- The bevel tip design is the only design that does not have an open lumen for tissue transport. The other two designs meet the demand of having an open lumen.
- The bending radius is a lot larger for the steering tip design than for the parallelogram-mechanism. This means that the parallelogram-mechanism bends more. The bending radius of the bevel tip design is very small. This makes sense as the maximum steering angle of this design is very small.
- Every design has a different shape at its tip: bevel, flat or conical.
- The design of the bevel tip only suffers from bifurcation as the cables in the parallelogram-mechanism are kept together in the tip.

From Table C.1 and the previous section, it is concluded that a combination of the parallelogram-mechanism and the steering cable design. Combining these two design will lead to a design with a large steering angle and an open lumen. Combining these design would include a design with four steering cables, which makes it easy to steer the flexible shaft. And using a lot of cables, as in the parallelogram-mechanism will make the shaft flexible and easy to bend.

D

Raw data

D.1. Experiment: Locomotion

Bending degree (Bending radius)	mm	cycles	mm/cycle
0° (infinity)	64	11	5.82
	72	11.5	6.26
	68	10.5	6.48
	77	12	6.42
	58	9.5	6.11
	59	10	5.90
15° (130mm)	67	15	4.47
	60	13	4.62
	34	8	4.25
	40	8	5.00
	52	10	5.20
	48	9	5.33
30° (105 mm)	50	9.5	5.26
	46	8	5.75
	39	7	5.57
	50	9	5.56
	62	10.5	5.90
	35	6	5.83
45°(80 mm)	49	10	4.90
	47	9	5.22
	57	11	5.18
	66	12	5.50
	61	12	5.08
	62	11.5	5.39

D.2. Experiment: Steerability

Wire rope	1	2	3	4
30 degrees	10,25	10,25	10,45	10,1
	10,75	10,2	9,05	10,7
	10,98	9,98	9,6	8,96
	11,05	9,99	9,6	10,5
	10,3	10,8	10,8	10,6
	11,52	10,52	9,8	9,6
60 degrees	14,2	13	14	13,7
	12,25	12,5	12,3	14
	13,95	14	12,1	13,7
	13,9	14,2	11,95	13,6
	12,4	12,7	14,2	14,1
	12,8	12,5	14,3	13
90 degrees	14,25	16,1	14,2	15,1
	13,7	14,75	13,75	16,2
	15,5	16,1	14,4	16,5
	13,8	13,95	13,75	15,5
	13,5	15,9	13,25	16,95
	16,4	16,3	13,95	17,8

E

Technical drawings

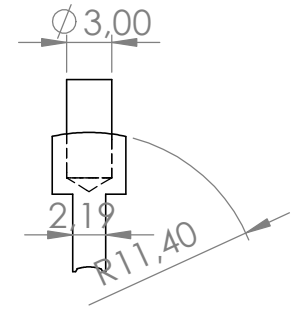

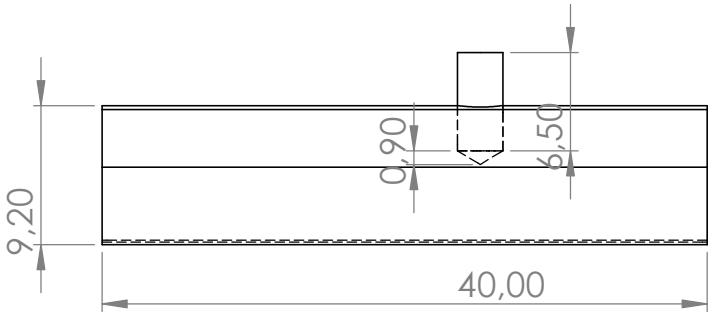

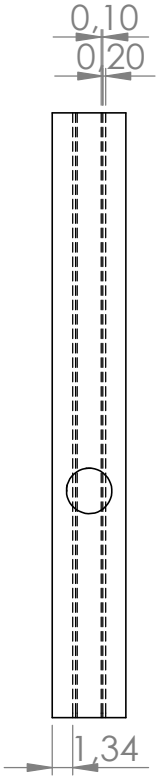

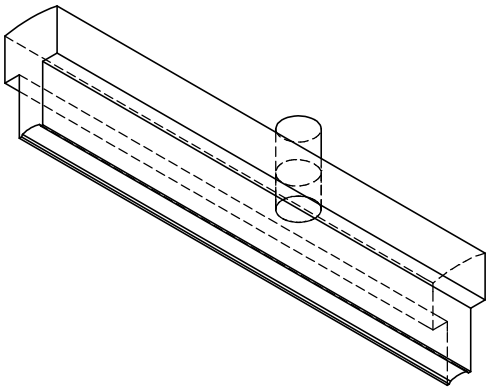

Drawn by Sanne Treep 19-02-2021	Drawing number: 2	TITLE: Inner slider
MATERIAL: Aluminium		A4
WEIGHT: 4.87 gram	SCALE:2:1	Unit of measure: mm

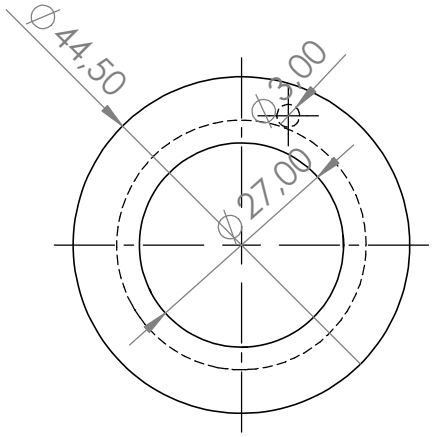

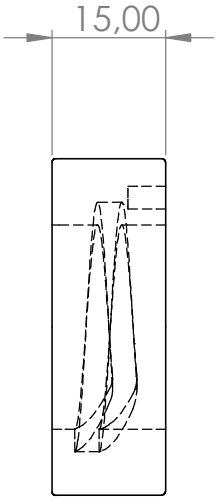

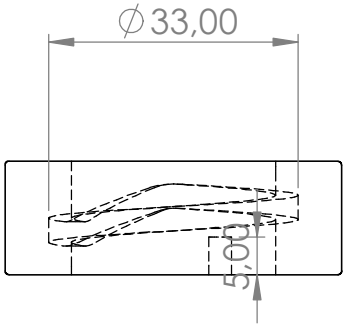

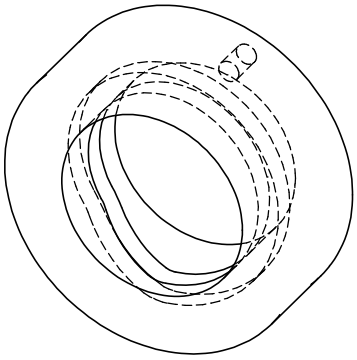

Drawn by Sanne Treep 19-02-2021	Drawing number: 3	TITLE: Inner cam
MATERIAL: ABS		A4
WEIGHT: 14 gram	SCALE:1:1	Unit of measure: mm

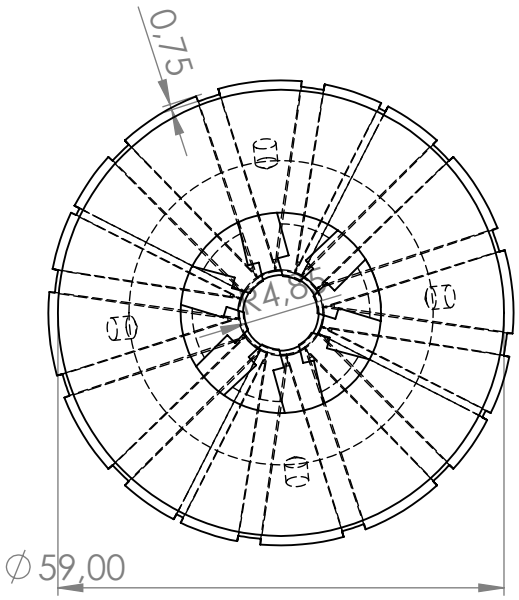

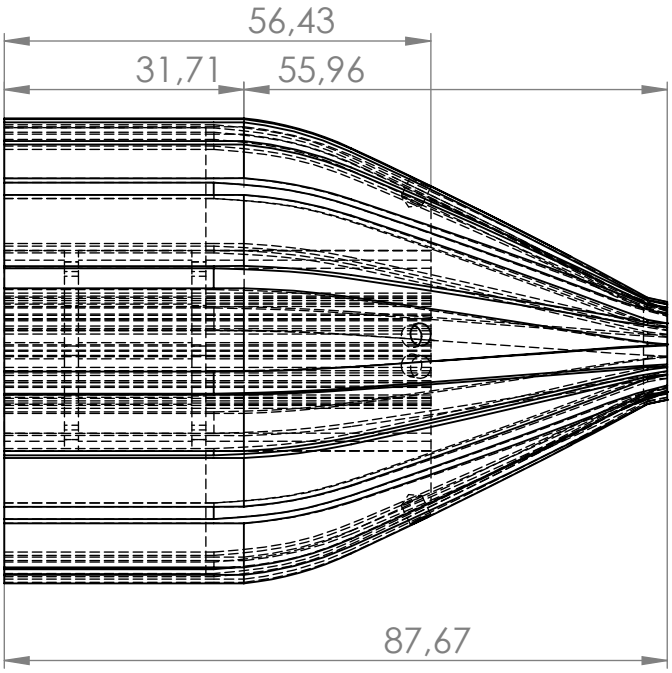

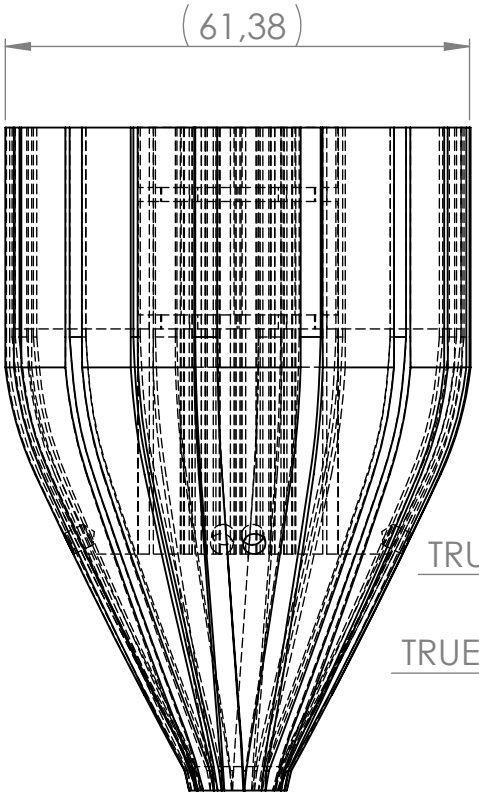

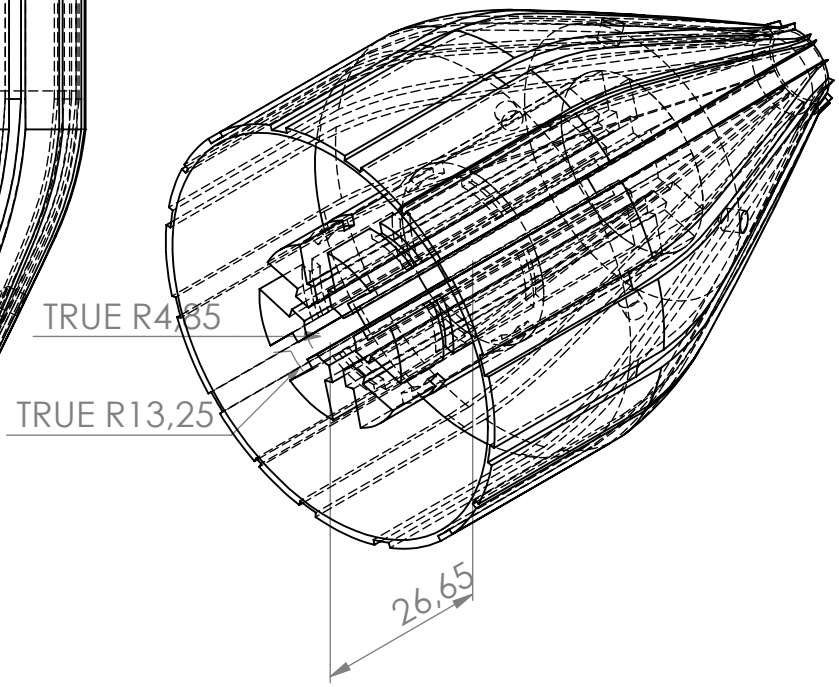

Drawn by Sanne Treep 19-02-2021	Drawing number: 4	TITLE: Inner cone
MATERIAL: ABS		A4
WEIGHT: 78.54 gram	SCALE:1:1	Unit of measure: mm

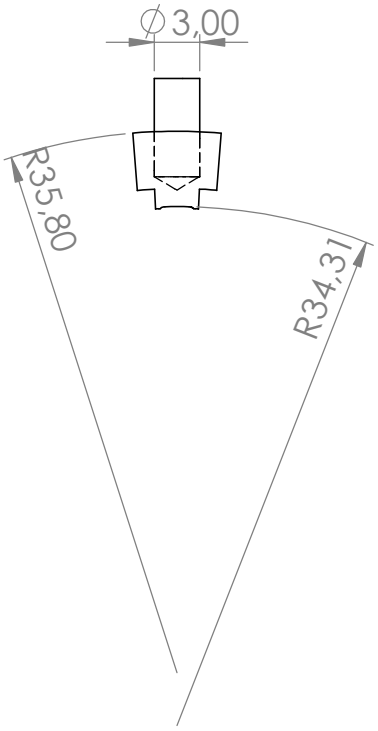

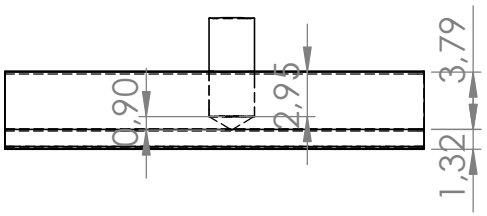

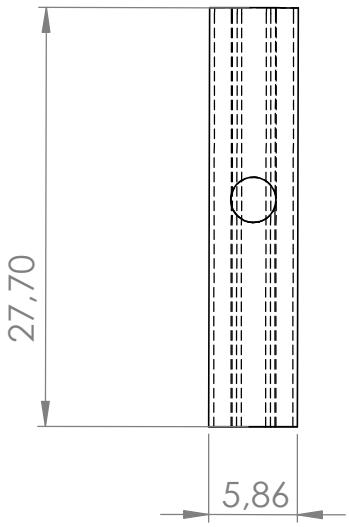

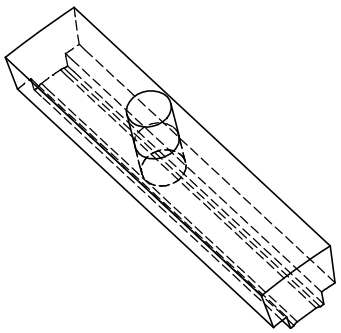

Drawn by Sanne Treep 19-02-2021	Drawing number: 5	TITLE: Outer slider
MATERIAL: Aluminium		A4
WEIGHT: 0.84 gram	SCALE:2:1	Unit of measure: mm

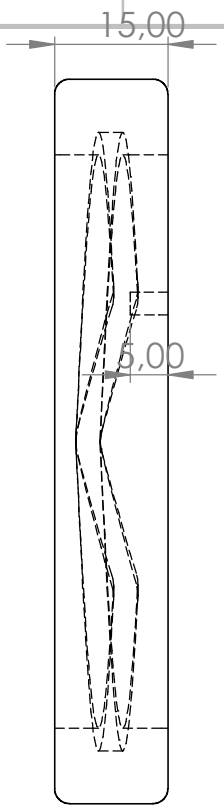

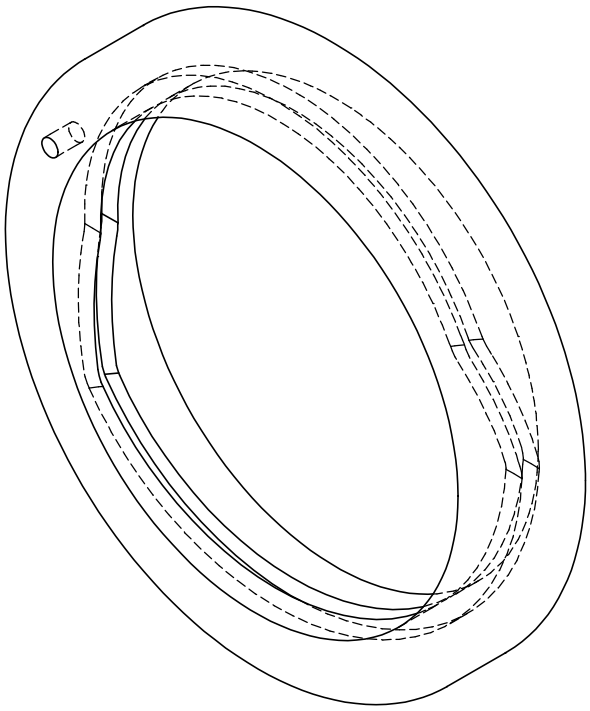

Drawn by Sanne Treep 19-02-2021	Drawing number: 6	TITLE: Outer cam
MATERIAL: ABS		A4
WEIGHT: 38.24 gram	SCALE:1:1	Unit of measure: mm

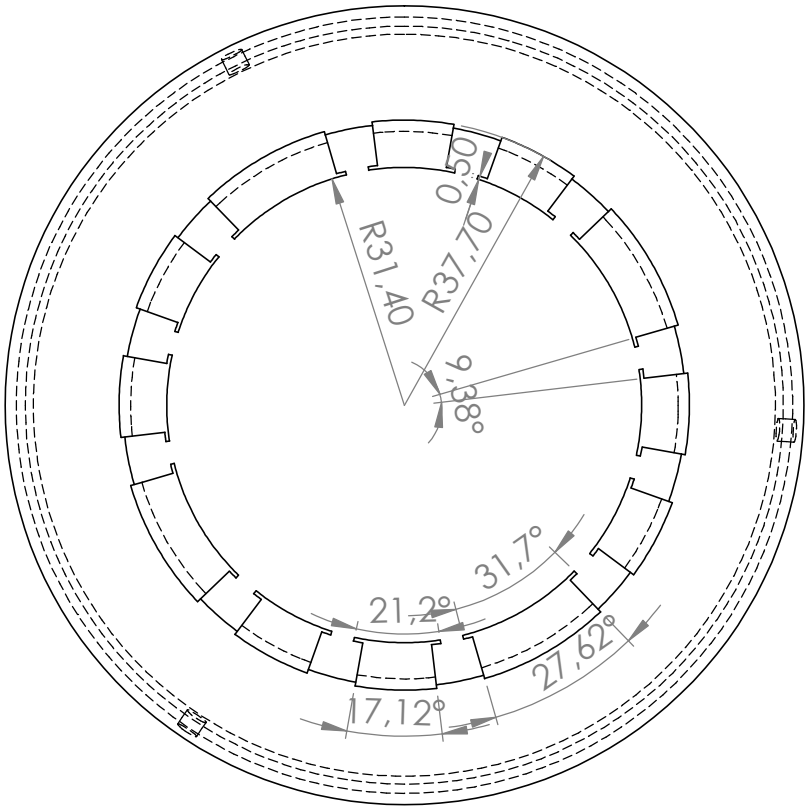

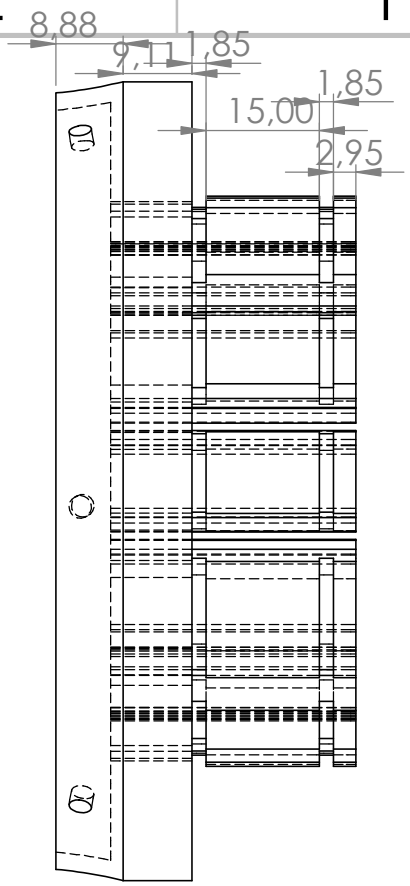

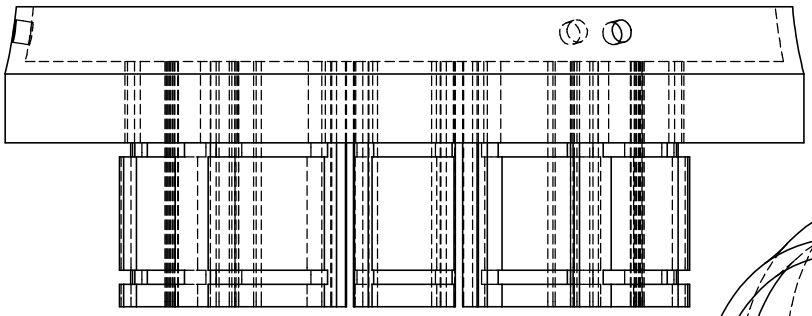

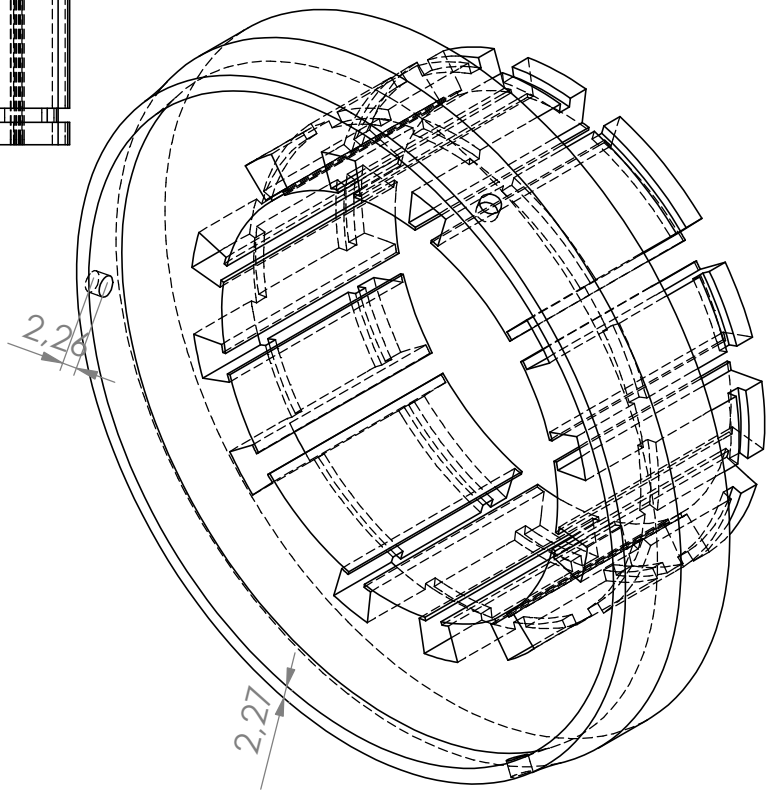

Drawn by Sanne Treep 19-02-2021	Drawing number: 7	TITLE: Slider house
MATERIAL: ABS		A4
WEIGHT: 82.65 gram	SCALE:1:1	Unit of measure: mm

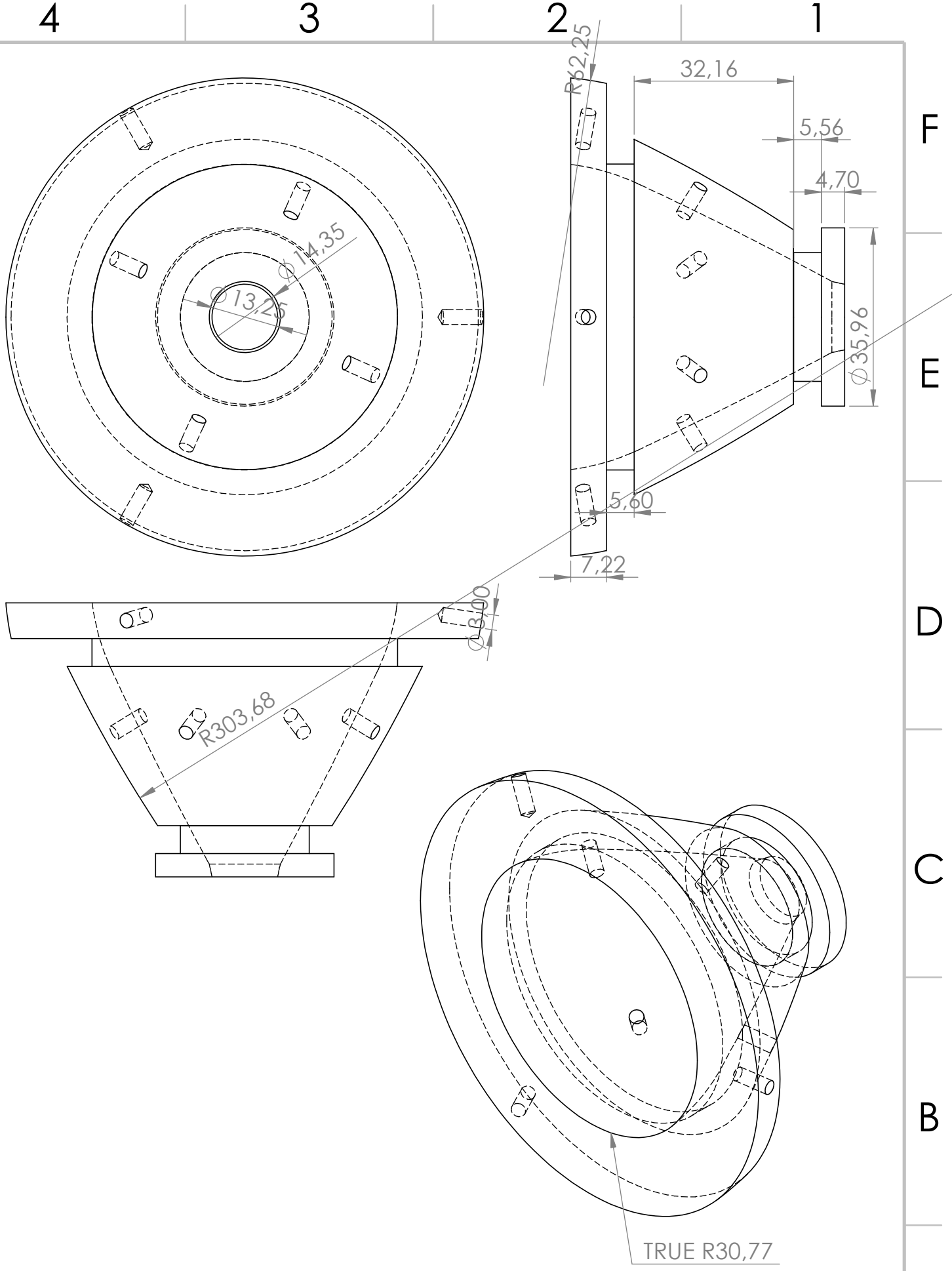

Drawn by Sanne Treep 19-02-2021	Drawing number: 8	TITLE: Outer cone
MATERIAL: ABS		A4
WEIGHT: 77.03 gram	SCALE:1:1	Unit of measure: mm

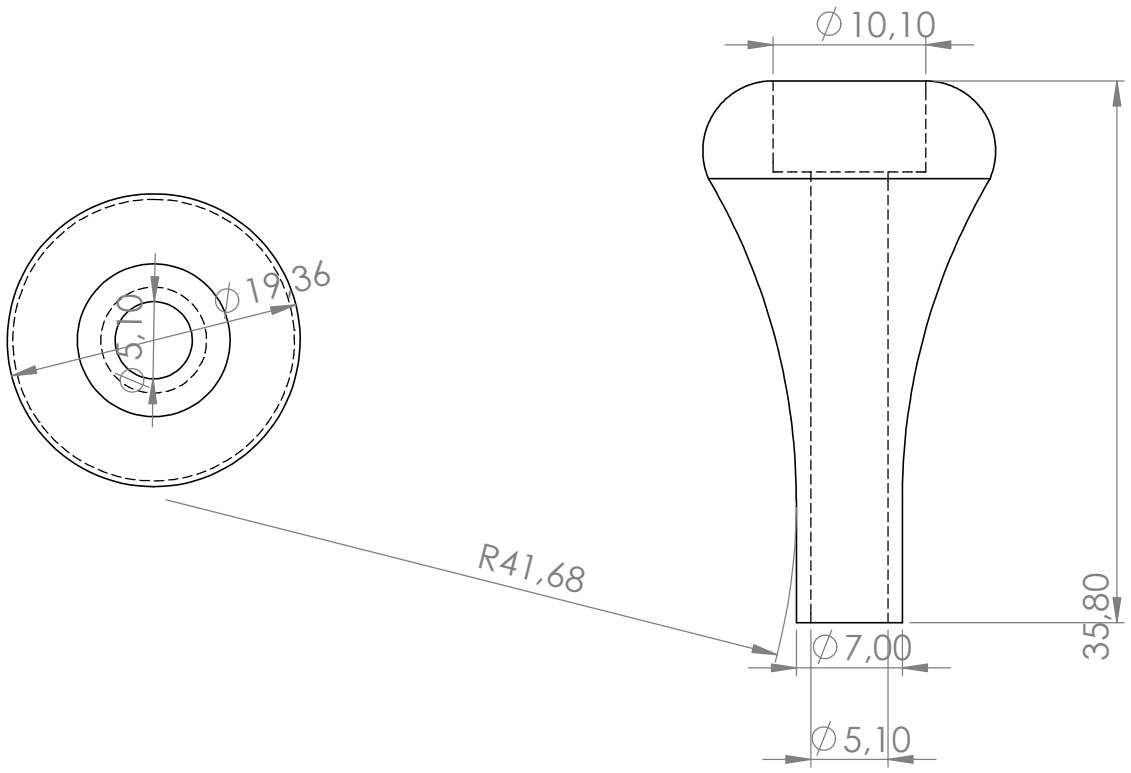

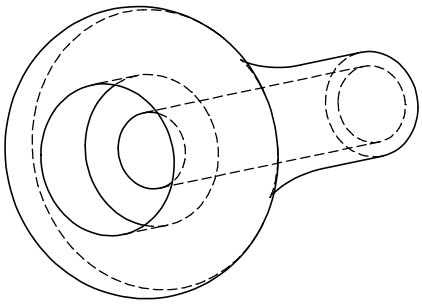

Drawn by Sanne Treep 19-02-2021	Drawing number: 9	TITLE: Inner sling
MATERIAL: ABS		A4
WEIGHT: 3 gram	SCALE:2:1	Unit of measure: mm

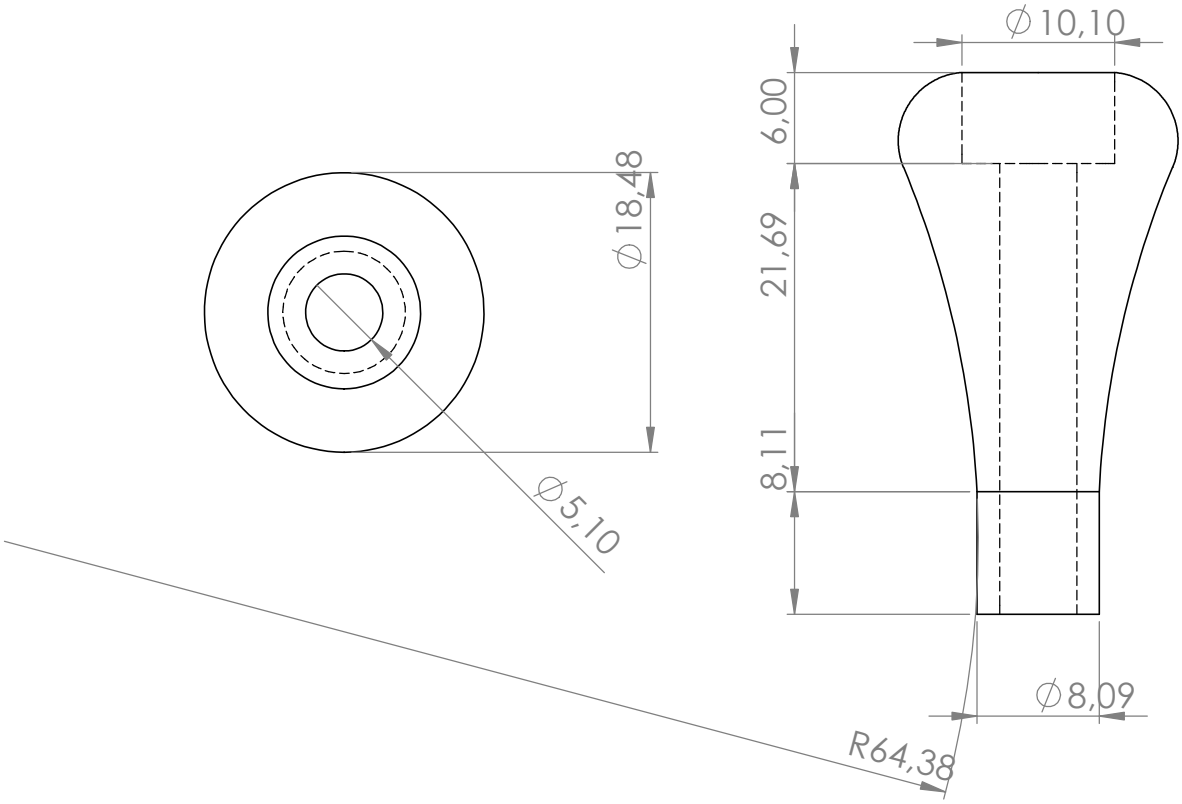

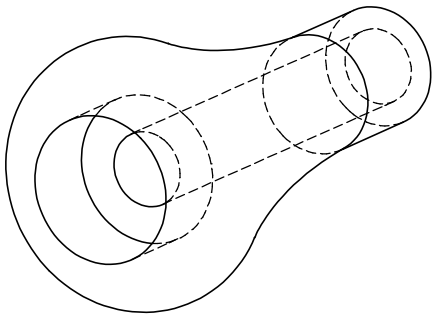

Drawn by Sanne Treep 19-02-2021	Drawing number: 10	TITLE: Outer sling
MATERIAL: ABS		A4
WEIGHT: 3 gram	SCALE:2:1	Unit of measure: mm

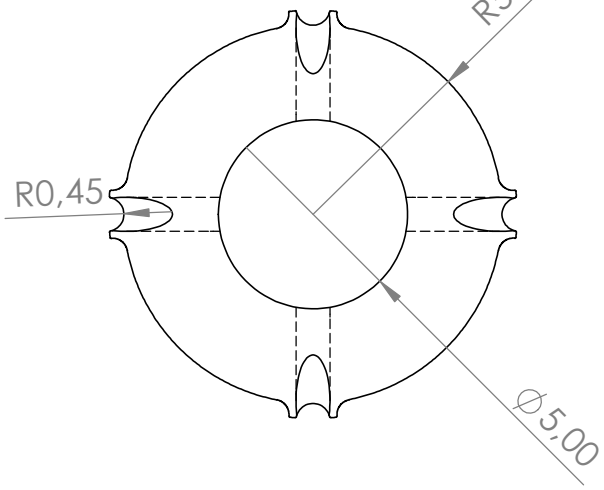

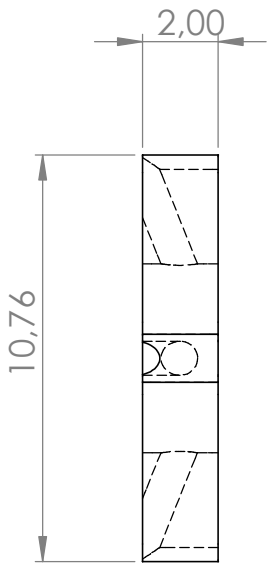

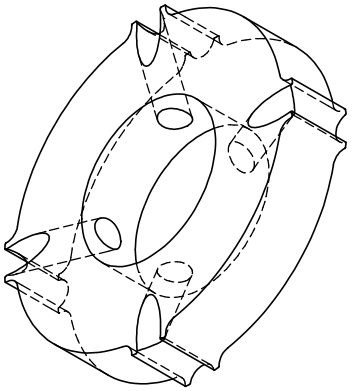

Drawn by Sanne Treep 19-02-2021	Drawing number: 1	TITLE: Tip
MATERIAL: Steel		A4
WEIGHT: 0.89 gram	SCALE:5:1	Unit of measure: mm

Bibliography

[1] Aquariumslang - 12/16 mm - transparant | Kunststof slangen | Leidingwerk & benodigdheden. URL https://zeeaquarium-winkel.nl/aquariumslang-12-16-mm-transparant.

[2] TRU COMPONENTS 1571490 Krimpkous zonder lijm Helder 12 mm Krimpverhouding: 3:1 per meter | MERCATEO. URL https://www.mercateo.nl/.

[3] A.D. Austin and T.O. Browning. A mechanism for movement of eggs along insect ovipositors. *International Journal of Insect Morphology and Embryology*, 10(2):93–108, 1981. ISSN 00207322. doi: 10.1016/S0020-7322(81)80015-3.

[4] T.H. Baron. Natural orifice transluminal endoscopic surgery. *British Journal of Surgery*, 94(1):1–2, 2007. ISSN 00071323. doi: 10.1002/bjs.5681. URL www.bjs.co.uk.

[5] G. Berci. Present and future developments in endoscopy. *Proceedings of the Royal Society of London. Series B. Biological Sciences*, 195(1119):235–242, 1977.

[6] P. Breedveld. Steerable Guidewire – Maneuvering without Twisting | BITE – Bio-Inspired Technology Group, 2010. URL https://www.bitegroup.nl/maneuverable-devices/steerable-guidewire/steerable-catheter/.

[7] P. Breedveld and J.S. Scheltes. Instrument for fine-mechanical or surgical applications. *WO 2005067785 (A1)*, jul 2005.

[8] P. Breedveld, J.S. Scheltes, E. M. Blom, and J.E.I. Verheij. A new, easily miniaturized steerable endoscope. *IEEE Engineering in Medicine and Biology Magazine*, 24(6):40–47, jul 2004. ISSN 07395175. doi: 10.1109/MEMB.2005.1549729.

[9] U. Cerkvenik, B. Van De Straat, S.W.S. Gussekloo, and J.L. Van Leeuwen. Mechanisms of ovipositor insertion and steering of a parasitic wasp. *Proceedings of the National Academy of Sciences of the United States of America*, 114(37):E7822–E7831, 2017. ISSN 10916490. doi: 10.1073/pnas.1706162114. URL www.pnas.org/cgi/doi/10.1073/pnas.1706162114.

[10] E. de Kater. The Design of a Flexible Friction-Based Transport Mechanism: A Bio-InspiredTransport Mechanism for Tissue Transport in Minimal Invasive Medical Interventions, 2020.

[11] D. Hellier, F. Albermani, B. Evans, H. De Visser, C. Adam, and J. Passenger. Flexural and torsional rigidity of colonoscopes at room and body temperatures. In *Proceedings of the Institution of Mechanical Engineers, Part H: Journal of Engineering in Medicine*, volume 225, pages 389–399, 2011. doi: 10.1177/09544119JEIM883.

[12] P. W. Henselmans, G. ; Smit, and P. Breedveld. Mechanical Follow-the-Leader. Institution of Mechanical Engineers. *Proceedings. Part H: Journal of Engineering in Medicine*, 233(11): 1141–1150, 2019. doi: 10.1177/0954411919876466. URL https://doi.org/10.1177/0954411919876466.

[13] S. Kawano, M. Kojima, Y. Higuchi, M. Sugimoto, K. Ikeda, N. Sakuyama, S. Takahashi, A. Hayashi, R.and Ochiai, and N. Saito. Assessment of elasticity of colorectal cancer tissue, clinical utility, pathological and phenotypical relevance. *Cancer Science*, 106(9):1232–1239, sep 2015. ISSN 13497006. doi: 10.1111/cas.12720. URL /pmc/articles/PMC4582994/?report=abstracthttps://www.ncbi.nlm.nih.gov/pmc/articles/PMC4582994/.

[14] A.J. Loeve. *Shaft-Guidance for Flexible Endoscopes*. PhD thesis, 2012. URL https://repository.tudelft.nl/islandora/object/uuid{%}3Af1f3782a-98b3-4e9a-b79a-00b210aecee3.

[15] J.D. Luketich, M. Alvelo-Rivera, P.O. Buenaventura, N.A. Christie, J.S. McCaughan, V.R. Litle, P.R. Schauer, J.M. Close, H.C. Fernando, and M.J. Zinner. Minimally Invasive Esophagectomy: Outcomes in 222 Patients. In *Annals of Surgery*, volume 238, pages 486–495. Lippincott, Williams, and Wilkins, oct 2003. doi: 10.1097/01.sla.0000089858.40725.68. URL /pmc/articles/PMC1360107/?report=abstracthttps://www.ncbi.nlm.nih.gov/pmc/articles/PMC1360107/.

[16] Mayo Clinic Staff. Colon polyps - Symptoms and causes - Mayo Clinic, 2017. URL https://www.mayoclinic.org/diseases-conditions/colon-polyps/symptoms-causes/syc-20352875.

[17] P. Posthoorn. The design of a self-propelling mechanism for an endoluminal robot. Technical report, 2017. URL http://repository.tudelft.nl/.

[18] D.J.L. Quicke and S.N. Ingram. Ovipositor structure and relationships within the Hymenoptera, with special reference to the Ichneumonoidea Numerical modeling of shelf seas View project Hymenoptera Phylogeny View project. *Article in Journal of Natural History*, 1994. doi: 10.1080/00222939400770301. URL http://dx.doi.org/10.1080/00222939400770301.

[19] D.K. Rex. Considering double contrast barium enema and its demise: A case for systematic videorecording of colonoscopy, dec 2008. ISSN 00029270. URL https://pubmed.ncbi.nlm.nih.gov/18853976/.

[20] W.O. Richards and D.W. Rattner. Endoluminal and transluminal surgery: No longer if, but when, apr 2005. ISSN 09302794. URL https://link.springer.com/article/10.1007/s00464-005-8100-9.

[21] M. Scali. Self-propelling needles From biological inspiration to percutaneous interventions. 2020. doi: 10.4233/uuid:523e3e5f-08f0-4acb-ab45-abaa7ace3967. URL https://doi.org/10.4233/uuid:523e3e5f-08f0-4acb-ab45-abaa7ace3967.

[22] M. Scali, T. P. Pusch, P. Breedveld, and D. Dodou. Ovipositor-inspired steerable needle: design and preliminary experimental evaluation. *Bioinspiration & Biomimetics*, 13(1):016006, dec 2018. ISSN 1748-3190. doi: 10.1088/1748-3190/AA92B9.

[23] N.J. van de Berg, J. Dankelman, and J.J. van den Dobbelsteen. Design of an actively controlled steerable needle with tendon actuation and FBG-based shape sensing. *Medical Engineering and Physics*, 37(6):617–622, jun 2015. ISSN 18734030. doi: 10.1016/j.medengphy.2015.03.016.

[24] I. van de Steeg. The Design of the Endo-Tubular Friction Carrier: A Bio-Inspired Alternative To Suction-Based Transport, 2018.

[25] D.A.K. Watters, A.N. Smith, M.A. Eastwood, K.C. Anderson, R.A Elton, and J.W. Mugerwa. Mechanical properties of the colon: Comparison of the features of the African and European colon in vitro. *Gut*, 26(4):384–392, 1985. ISSN 00175749. doi: 10.1136/gut.26.4.384. URL http://gut.bmj.com/.